NASA CONTRACTOR REPORT

NASA CR-2

NASA CR-2889

THE LINEAR FRESNEL LENS SOLAR CONCENTRATOR: TRANSVERSE TRACKING ERROR EFFECTS

Robert M. Cosby

Prepared by
BALL STATE UNIVERSITY
Muncie, Ind.
for George C. Marshall Space Flight Center

NATIONAL AERONAUTICS AND SPACE ADMINISTRATION • WASHINGTON, D. C. • AUGUST 1977

1. REPORT NO.	2. GOVERNMENT ACCESSION NO.	3. RECIPIENT
NASA CR-2889		

4. TITLE AND SUBTITLE	5. REPORT DATE
The Linear Fresnel Lens Solar Concentrator: Transverse Tracking Error Effects	August 1977
	6. PERFORMING ORGANIZATION CODE
7. AUTHOR(S)	8. PERFORMING ORGANIZATION REPORT #
Robert M. Cosby	M-228
9. PERFORMING ORGANIZATION NAME AND ADDRESS	10. WORK UNIT NO.
Department of Physics and Astronomy Ball State University Muncie, Indiana	11. CONTRACT OR GRANT NO. NCA8-00121, Mod 3
	13. TYPE OF REPORT & PERIOD COVERED
12. SPONSORING AGENCY NAME AND ADDRESS	Contractor Report
National Aeronautics and Space Administration Washington, D. C. 20546	14. SPONSORING AGENCY CODE

15. SUPPLEMENTARY NOTES

16. ABSTRACT

Real sun-tracking linear solar concentrators imperfectly follow the solar disc, operationally sustaining both transverse and axial misalignments. This report details an analysis of the solar concentration performance of a line-focusing, flat base Fresnel lens in the presence of small transverse tracking errors. Simple optics and ray-tracing techniques are used to evaluate the lens solar transmittance and focal plane imaging characteristics. Solar transmission losses by Fresnel reflection and material absorption are included and an analysis of groove edge losses is presented. Computer-generated example data are presented for lenses with parameters corresponding to two NASA test articles: a 0.56 m wide, f/1.0 lens and a 1.83 m wide, f/0.9 lens. Results indicate less than a 1 percent transmittance degradation for transverse errors up to 2.5^0. In this range, solar image profiles shift laterally in the focal plane, the peak concentration ratio drops, and profile asymmetry increases with tracking error. With profile shift as the primary factor, the ninety percent target intercept width increases rapidly for small misalignments, e.g., almost threefold for a 1^0 error for the small test lens. The analytical model and computational results provide a design base for tracking and absorber systems for the Fresnel lens solar concentrator.

17. KEY WORDS	18. DISTRIBUTION STATEMENT
	STAR Category: 44

19. SECURITY CLASSIF. (of this report)	20. SECURITY CLASSIF. (of this page)	21. NO. OF PAGES	22. PRICE
Unclassified	Unclassified	54	$4.50

*For sale by the National Technical Information Service, Springfield, Virginia 22161.

CONTENTS

NOMENCLATURE

Symbol	Definition
A	total transmitted fraction of incident sunlight
A_j	transmission for jth wavelength interval
F_u, F_ℓ	fractions of incident sunlight lost to groove blocking in upper and lower lens halves, respectively
f	lens focal length
$I(Y)$	total intensity at position Y
$I_j(Y)$	jth wavelength intensity at Y
i	serration index
j	wavelength index
L, L_{ij}	beam spread for sunlight within jth wavelength interval refracted from ith serration
$\Delta\ell$	defocus length parameter
N	design index of refraction
n	index of refraction
q	incident solar intensity
r_i, s_i	ray-lens geometrical parameters; refer to ray diagrams
T_a	bulk transmittance factor
T_1	transmittance of surface 1
T_2	transmittance of surface 2
T, T_{ij}	transmittance through ith serration for sunlight within jth wavelength interval
$T_i(y)$	sunlight transmittance of ith serration
T_s	groove blocking transmittance factor
t	lens thickness

W	lens width
y	serration position variable with respect to lens axis
$(\Delta y)_i$	serration width
Y	position variable with respect to length axis of lens and in a plane parallel to and beneath the concentrator
$Y_r, Y_\ell, Y_{ru}, Y_{r\ell}$	extreme ray intercepts
2α	apparent angular diameter of the sun
$\alpha_1', \alpha_2', \alpha_3'$	extreme ray refraction angles at first lens surface
γ_1-γ_7	angles between the emergent refracted extreme rays and the normal to the plane of the lens
δ	transverse error angle
Θ, Θ_i	groove angle for ith serration
λ, λ_j	wavelength
ϕ_i, ϕ_i'	angles of incidence
ϕ_t, ϕ_t'	angles of refraction
ω_j	solar flux weighting factor

LIST OF ILLUSTRATIONS

LIST OF ILLUSTRATIONS (Cont.)

I. INTRODUCTION

The economics of tracking systems for solar concentrators depend directly on the precision demanded in following the solar disc. The required precision is determined by the concentrator's performance sensitivity to tracking errors and by the concentration requirements of a particular application. Specified energy collection conditions are achieved by appropriate design of a primary concentrator-absorber system or primary concentrator-secondary concentrator-absorber system. Such design is possible only if the solar imaging and flux transferral (transmission/reflection) properties of the primary concentrator are known for a variety of conditions, including imperfect sun tracking. Design and optimum placement of a secondary concentrator and/or absorber require an evaluation of the concentrator imaging sensitivity to defocusing.

An economically attractive concentrator of the refractor type for medium concentration applications is the linear flat base Fresnel lens. The solar concentration characteristics, including defocusing sensitivities, of a perfectly tracking, line focusing Fresnel lens have been analyzed during this study and reported in detail in Reference [1]. In actual concentrator operation, both axial and transverse tracking errors will occur. A general objective of the present project is to examine the effects on performance of a transverse tracking error for this type of solar concentrator using simple optical analysis, ray tracing techniques, and computer generation of example data. Zero axial alignment error is assumed and all incident solar rays are approximated as having no axial component. Specific objectives are to compute the lens transmittance degradation and the image profile shift and distortion under small transverse tracking error conditions ($\leq 2.5°$) for two NASA test articles: a 56 cm wide, f/1.0 and a 1.83 meter wide, f/0.9 lens.

II. THEORY

The solar transmission and concentration characteristics of a Fresnel lens with a small transverse tracking error ($\leq 2.5°$) are studied using optical ray trace techniques similar to those in previous analysis for a perfectly tracking concentrator [1,2,3]. The major change occurs in the loss of symmetry about the lens axis. The lens is assumed to have a compression molded geometry and to be free of manufacturing defects, wind load, and thermal expansion effects. Other assumptions include:

- The height of a serration on the lens is much less than the focal length.
- Diffraction by groove edges is negligible.
- Any anomalous dispersion effects near absorption bands in the acrylic have negligible effect.
- The sun is a uniform source of radiation.
- The solar flux refracted by a single serration is uniformly distributed over the beam spread width in the intercept plane beneath the lens.
- Lens orientation in the seasonal (longitudinal) direction is perfect; solar rays are approximated as having no axial components.

A. Transmission Characteristics

Following a previous analysis [1], the total transmission coefficient is written as a product:

$$T = T_1 T_a T_2 T_s, \tag{1}$$

with T_1 the Fresnel transmittance factor for the first lens surface, T_a a bulk transmittance factor, T_2 the Fresnel factor for the second surface, and T_s a "shading" factor. While the empirical treatment of absorption (T_a) is unchanged, the Fresnel factor $T_1 T_2$ is now evaluated for rays from the sun's center incident at an

angle δ, the transverse error angle, rather than for rays normal to the lens surface.

The transmissivity for natural light incident at the boundary between two optical media is given by

$$T(\phi_i,\phi_t) = \frac{\sin 2\phi_i \sin 2\phi_t \left[1 + \sec^2 (\phi_i - \phi_t)\right]}{2 \sin^2(\phi_i + \phi_t)} \tag{2}$$

where ϕ_i and ϕ_t are the angles of incidence and refraction, respectively. Referring to Figure 1(a) and using Snell's law of refraction, the angles for the first surface are

$$\begin{aligned} \phi_i &= \delta \\ \phi_t &= \text{Arcsin } (\tfrac{\sin\delta}{n}), \end{aligned} \tag{3}$$

where n is the appropriate index of refraction.

For the serrated surface on the "upper" half of the lens, the incident angle ϕ_i' and refraction angle ϕ_t' are (Figure 1(a))

$$\begin{aligned} \phi_i' &= \theta + \phi_t \\ \phi_t' &= \text{Arcsin } (n \sin \phi_i'), \end{aligned} \tag{4}$$

and for the "lower" half (Figure 1(b))

$$\phi_i' = |\theta - \phi_t|, \tag{5}$$

with ϕ_t' as above.

Here θ is the groove angle given by [1]

$$\theta = \text{Arctan} \left\{ \frac{y}{N\left[y^2 + (f-t)^2 \right]^{\frac{1}{2}} - (f-t)} \right\} \tag{6}$$

with y the serration distance from the lens centerline, f the focal length, t the lens center thickness, and N the design index of refraction.

Thus the product T_1T_2 can be evaluated from

$$\begin{aligned} T_1 &= T(\phi_i, \phi_t), \\ T_2 &= T(\phi_i', \phi_t'), \end{aligned} \tag{7}$$

and the above equations.

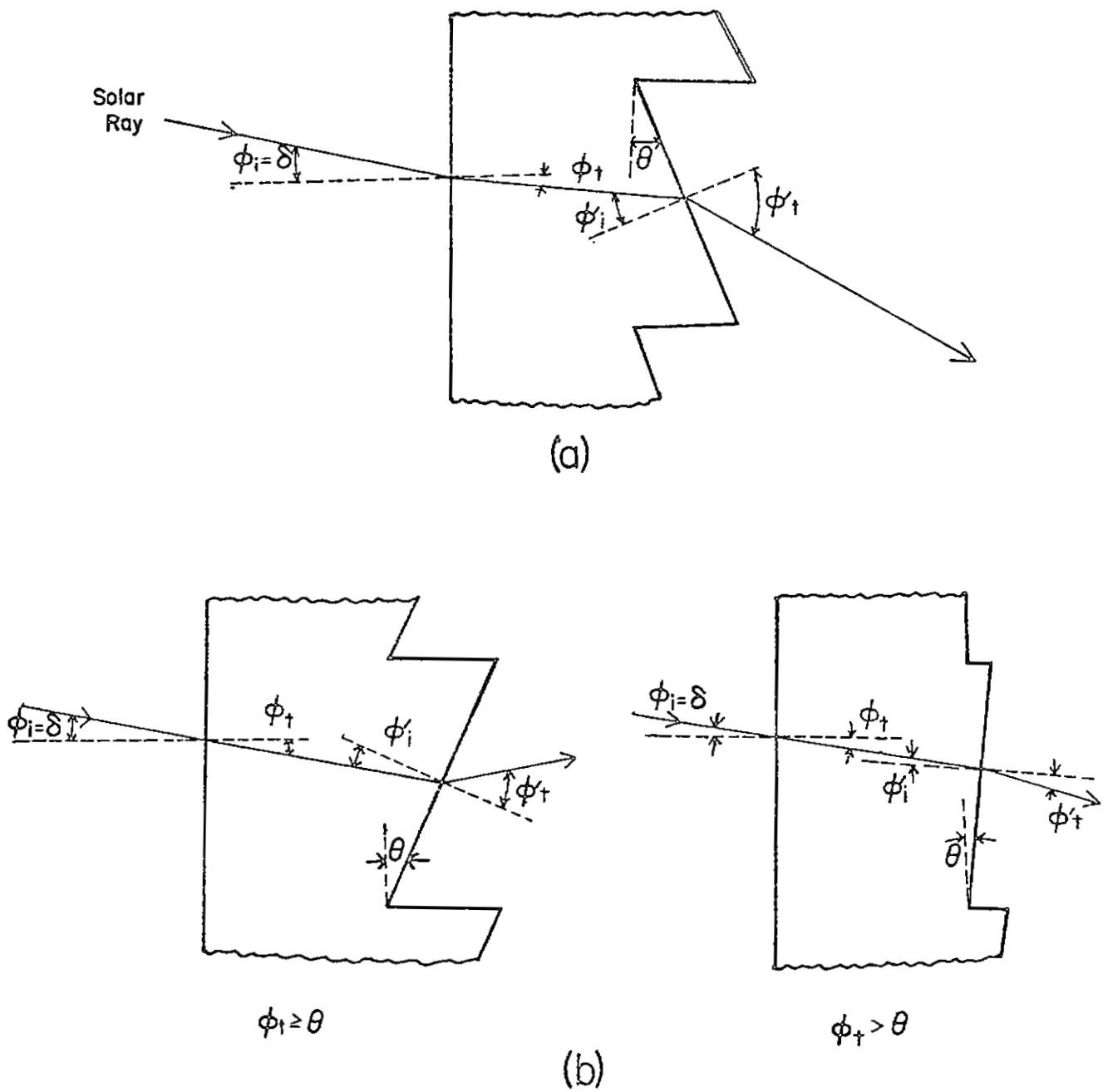

Figure 1. Refraction of rays from center of sun.

Rays of sunlight incident on a serration may be refracted such that they either strike the serration edge surface or, after passing thru the lens, are obstructed by an adjacent serration. In this analysis such rays are assumed lost, i.e., do not contribute to the intensity profile in an image plane below the lens. Since the step heights are diminutive and the transverse error is assumed small, the losses are also expected minor.

As depicted in Figures 2 and 3 for the upper and lower lens halves, respectively, various possible "shading" cases for incident sunlight must be considered. The method of analysis for the fractions, F_u and F_ℓ, of incident light lost thru the various illustrated cases for a given serration (the ith) and for a particular wavelength is outlined in the Appendix. The results are summarized below:

CASE: Figure 2(a), upper half.

$$F_u' \simeq \frac{\delta \tan\theta_i}{n}, \qquad \delta \geq \alpha \tag{8}$$

$$F_u' \simeq \frac{(\delta + \alpha)^2 \tan\theta_i}{4\alpha n}, \qquad \delta < \alpha. \tag{9}$$

CASE: Figure 2(b), upper half.

$$F_u'' = 0, \qquad \delta \geq \alpha \tag{10}$$

$$F_u'' \simeq \frac{\tan\theta_{i+1}}{4\alpha}[\alpha - \delta + (2-n)\theta_i](\alpha - \delta - n\theta_i), \tag{11}$$

$$\text{for } \delta < \alpha \text{ and } n\theta_i \leq \alpha - \delta$$

$$F_u'' = 0 \qquad \text{for } \delta < \alpha \text{ and } n\theta_i > \alpha - \delta. \tag{12}$$

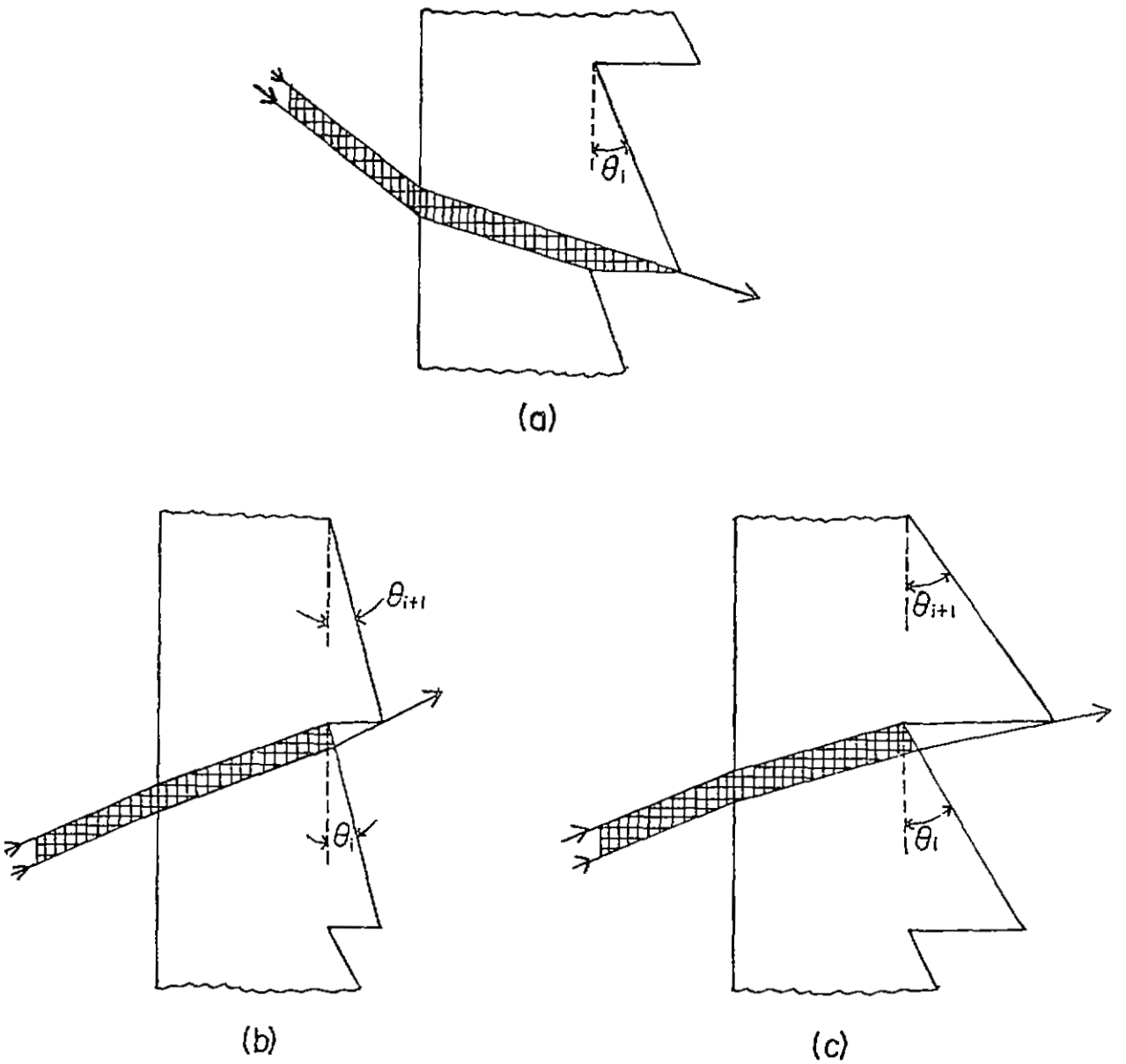

Figure 2. Groove edge losses for upper lens half.

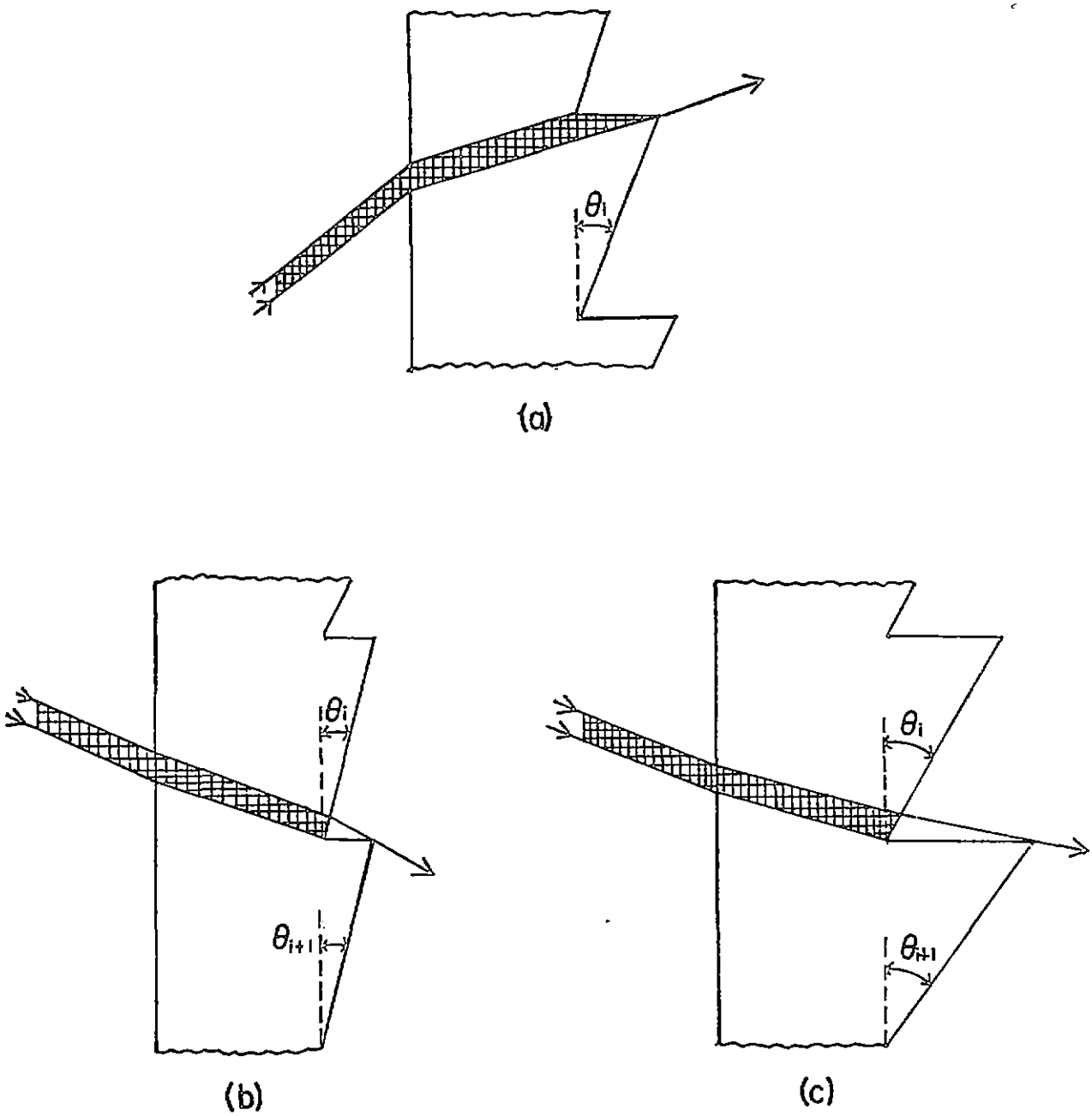

Figure 3. Groove edge losses for lower lens half.

CASE: Figure 2(c), upper half.

$$F_u''' = 0, \qquad \delta \geq \alpha \ ; \tag{13}$$

$$F_u''' \simeq \frac{\tan \theta_{i+1}}{2\alpha n} \ nAB(\alpha - \delta - \phi_{io}) + \frac{A^2}{2} [(\alpha - \delta)^2 - \phi_{io}^2]$$

$$+ \left[\frac{AB\phi_{io} + n(B^2 + 1)}{2B}\right]\rho(\phi_{io}) - \left[\frac{AB(\alpha - \delta) + n(B^2 + 1)}{2B}\right]\rho(\alpha - \delta)$$

$$- \left[\frac{2n^2A^2(AB^2 - 1) - 1}{2B^2}\right]\sigma(\alpha - \delta) \quad ,$$

$$\text{for } \delta < \alpha, \tag{14}$$

and where

$$A = \sin \theta_i \ ; \tag{15}$$

$$B = \cos \theta_i \ ; \tag{16}$$

$$\phi_{io} = \text{Arcsin} \{ n \sin [\theta_i - \text{Arcsin} (\frac{\sin \theta_i}{n})]\} \ ; \tag{17}$$

$$\rho(\chi) \equiv \sqrt{(1 - n^2A^2) + (2n\,AB)\chi - (B^2)\chi^2} \ ; \tag{18}$$

$$\sigma(\chi) \equiv \frac{1}{B}\{\text{Arcsin}[B\chi - nA] - \text{Arcsin}\,(B\phi_{io} - nA)\} \ . \tag{19}$$

CASE: Figure 3(a), lower half.

$$F_\ell' = 0 \ , \qquad \delta \leq \alpha \ ; \tag{20}$$

$$F_\ell' \simeq \frac{(\alpha - \delta)^2 \tan\theta_i}{4\alpha n}, \qquad \delta < \alpha. \tag{21}$$

CASE: Figure 3(b), lower half.

$$F_\ell'' = \frac{\tan\theta_{i+1}}{4\alpha} (\delta + \alpha - n\theta_i)[\delta + \alpha + (2 - n)\theta_i] \ , \tag{22}$$

$$n\theta_i < \delta + \alpha \ ;$$

$$F_\ell'' = 0 \ , \ n\theta_i \geq \delta + \alpha \ . \tag{23}$$

LIST OF TABLES

CASE: Figure 3(c), lower half.

$$F_{\ell}'' = \frac{\tan\theta_{i+1}}{2\alpha n} nAB(\alpha + \delta - \phi_{io}) + \frac{A^2}{2}\left[(\alpha + \delta)^2 - \phi_{io}^2\right]$$

$$+\left[\frac{AB\phi_{io} + n(B^2 + 1)}{2B}\right] \rho(\phi_{io}) - \left[\frac{AB(\alpha + \delta) + n(B^2 + 1)}{2B}\right] \rho(\alpha + \delta)$$

$$-\left[\frac{2n^2A^2(AB^2 - 1) - 1}{2B^2}\right] \sigma(\alpha + \delta) ,$$

for $n\theta_i > \delta + \alpha$, and (24)

$$F_{\ell}''' = \frac{\tan\theta_{i+1}}{2\alpha n} nAB(n\theta_i - \phi_{io}) + \frac{A^2}{2}(n^2\theta_i^2 - \phi_{io}^2)$$

$$+\left[\frac{AB\phi_{io} + n(B^2 + 1)}{2B}\right] \rho(\phi_{io}) - \left[\frac{ABn\theta_i + n(B^2 + 1)}{2B}\right] \rho(n\theta_i)$$

$$- \frac{2n^2A\ (AB^2 - 1) - 1}{2B^2} \sigma(n\theta_i) , \quad \text{for } \delta + \alpha > n\theta_i. \quad (25)$$

The lost fraction of incident light is

$$F_u = F_u' + F_u'' + F_u'' , \quad (26)$$

$$F_{\ell} = F_{\ell}' + F_{\ell}'' + F_{\ell}''' ,$$

for the upper and lower serrations, respectively.

Then

$$T_s = 1 - F_u \quad \text{(upper)}$$

and (27)

$$T_s = 1 - F_{\ell} \quad \text{(lower)} .$$

The transmission coefficient evaluated from Equation (1) may be used to calculate the serration transmission $T_i(y)$ as a function of serration position, the fraction A_j transmitted for one wavelength interval, and the total sunlight transmittance A:

$$T_i(y) = \sum_j \omega_j \, T_{ij}(y) \ , \tag{28}$$

$$A_j = \frac{1}{W} \sum_i T_{ij} \, (\Delta y)_i \ , \tag{29}$$

$$A = \sum_j \omega_j \, A_j \ . \tag{30}$$

The ω_j are spectral weighting factors, W is the lens width, $(\Delta y)_i$ the serration width, and the summations, $(\sum_i)$ and $(\sum_j)$, are over all lens serrations and all solar wavelengths[1]. In deriving the above equations, the decrease in incident flux caused by the small tracking error is assumed negligible since the cosδ factor is essentially 1.00 for all errors studied.

B. Concentrated Flux Distribution

The local concentration ratio in an image plane below the lens is given by [1]

$$\frac{I(Y)}{q} = \sum_j \frac{I_j(Y)}{q} = \sum_j \sum_i \frac{\omega_j \, T_{ij} \, (\Delta y)_i}{L_{ij}} \ , \tag{31}$$

with L_{ij} the beam spread width. Now

$$L = Y_r - Y_\ell \ , \tag{32}$$

where Y_r and Y_ℓ are the extreme ray intercepts in the image plane for light exiting a serration. Determination of these intercepts for all serrations in the presence of a transverse tracking error

constitutes the balance of the analysis. The study of refraction of extreme rays is divided by considering separately the upper and lower lens halves and subdivided according to the magnitude of the tracking error compared to the angle (2α) subtended by the solar disc.

1. Upper Half of Lens

   a. $\delta \geq \alpha$

   Extreme rays exiting at the serration edges are depicted in Figure 4. For this case,

$$Y_{ru} = y_i + \frac{(\Delta y)_i}{2} - (f + \Delta\ell - t) \tan \gamma_1 , \qquad (33)$$

$$Y_{\ell u} = y_i - \frac{(\Delta y)i}{2} - (f + \Delta\ell - t - (\Delta y)_i \tan\theta_i)\tan\gamma_2, \qquad (34)$$

   where $\Delta\ell$ is a defocus parameter and γ_1, γ_2 are ray exit angles. Applying Snell's law at the two surfaces.

$$\gamma_1 = \text{Arcsin } [n \sin (\alpha_1' + \theta_i)] - \theta_i ; \qquad (35)$$

$$\gamma_2 = \text{Arcsin } [n \sin (\alpha_2' + \theta_i] - \theta_i ; \qquad (36)$$

   where

$$\alpha_1' = \text{Arcsin } \left[\frac{\sin (\delta - \alpha)}{n}\right] , \qquad (37)$$

   and

$$\alpha_2' = \text{Arcsin } \left[\frac{\sin (\delta + \alpha)}{n}\right] . \qquad (38)$$

   b. $\delta < \alpha$

   For this case, the ray determining Y_ℓ is identical to that in Figure 4. Hence Y_ℓ is given by Equation (34). Figures 5(a), (b), and (c) illustrate three possible refraction scenarios for the ray determining Y_r depending on the groove angle and the ray position with respect to the serration normal at the grooved surface.

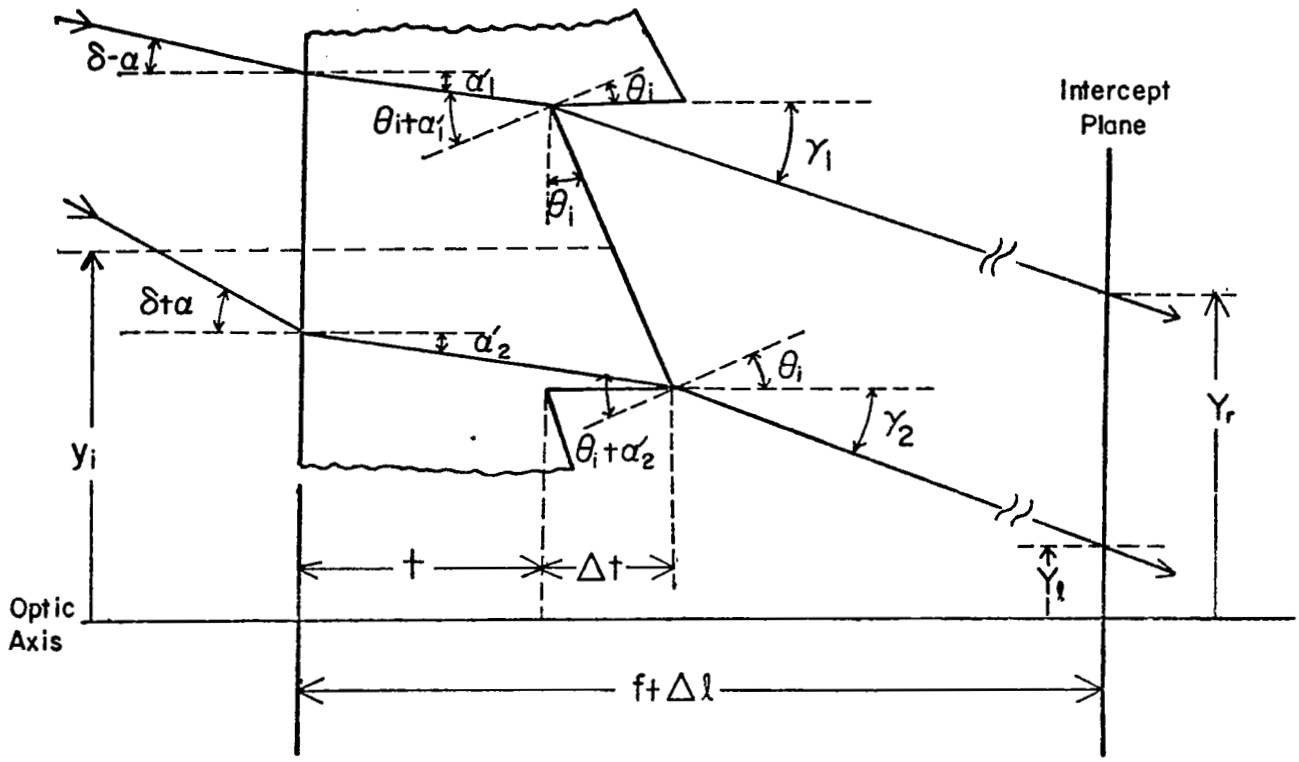

Figure 4. Extreme ray paths in upper lens half serrations; $\delta > \alpha$.

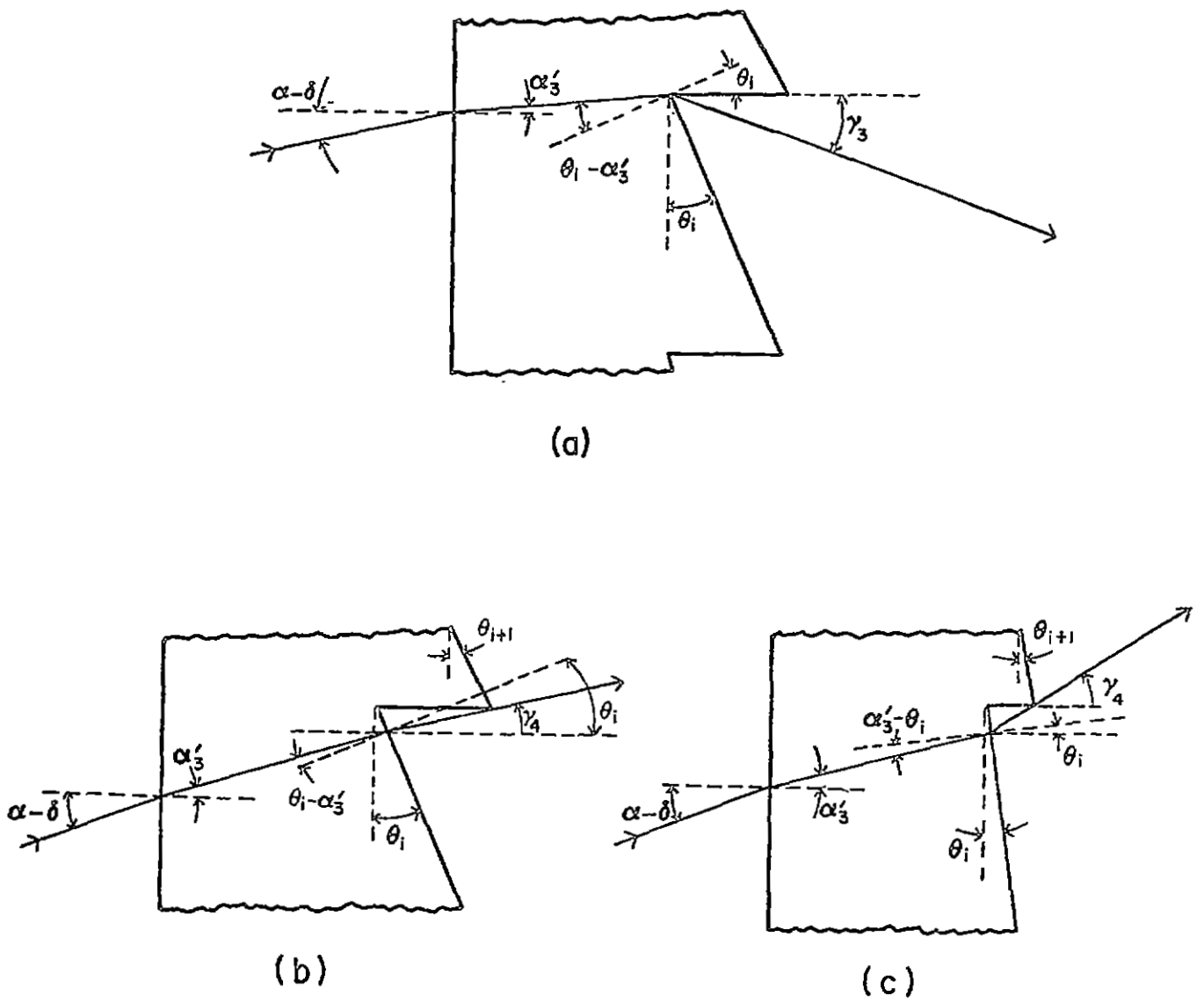

Figure 5. Extreme ray paths in upper lens half serrations; $\delta < \alpha$.

For the situation in Figure 5(a),

$$Y_{ru} = y_i + \frac{(\Delta y)_i}{2} - (f + \Delta\ell - t) \tan \gamma_3 \ , \tag{39}$$

$$\gamma_3 + \text{Arcsin}\,[n \sin (\theta_i - \alpha_3')] - \theta_i \ , \tag{40}$$

and

$$\alpha_3' = |\alpha_1'| \ . \tag{41}$$

For the rays in Figure 5(b) and 5(c) ,

$$Y_{ru} = y_i + \frac{(\Delta y)_i}{2} + \left[f + \Delta\ell - t - (\Delta y)_i \tan\theta_{i+1}\right] \tan \gamma_4, \tag{42}$$

where

$$\gamma_4 = - \gamma_3 \ . \tag{43}$$

2. Lower Half of Lens

a. $\delta \geq \alpha$

Figure 6(a) and 6(b) display possible ray paths determining the intercept Y_r for serrations in the lower lens half. With the aid of Figure 6(a),

$$Y_{rb} = - \left[y_i - \frac{(\Delta y)_i}{2} + r_i - (f + \Delta\ell - t - s_i) \tan \gamma_5\right] \ , \tag{44}$$

where

$$\gamma_5 = \text{Arcsin}[n \sin(\theta_i - \alpha_1')] - \theta_i \ , \tag{45}$$

$$r_i = s_i \tan \alpha_1' \ , \tag{46}$$

and

$$s_i = \frac{(\Delta y)_i \tan \theta_i}{1 + \tan \alpha_1' \tan \theta_i} \ . \tag{47}$$

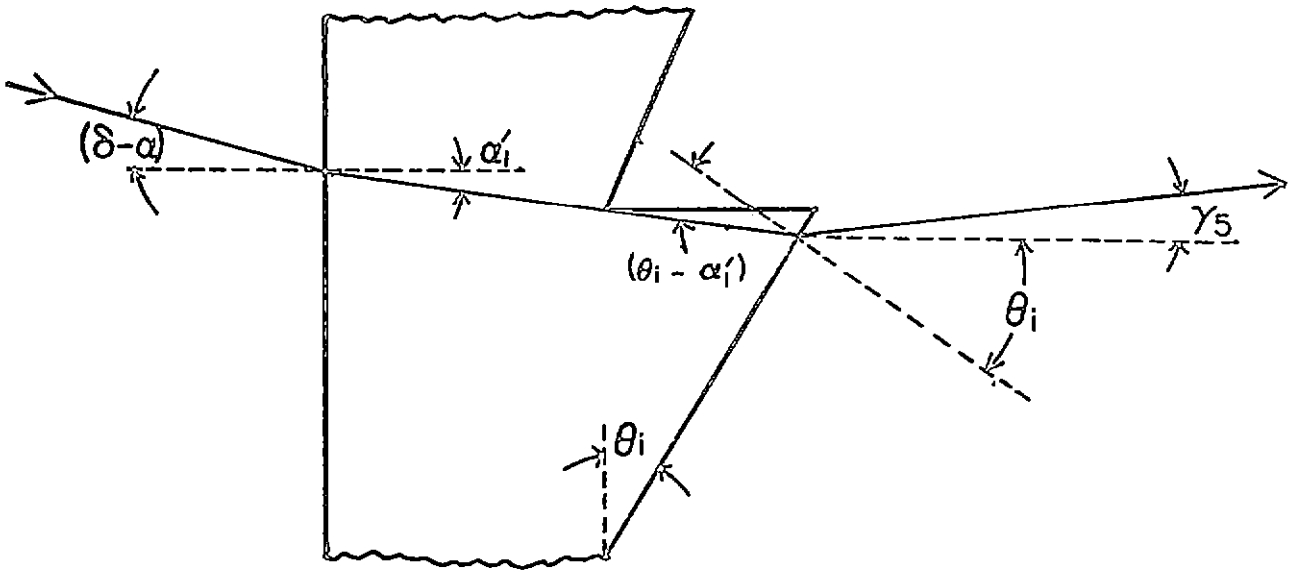

(a)

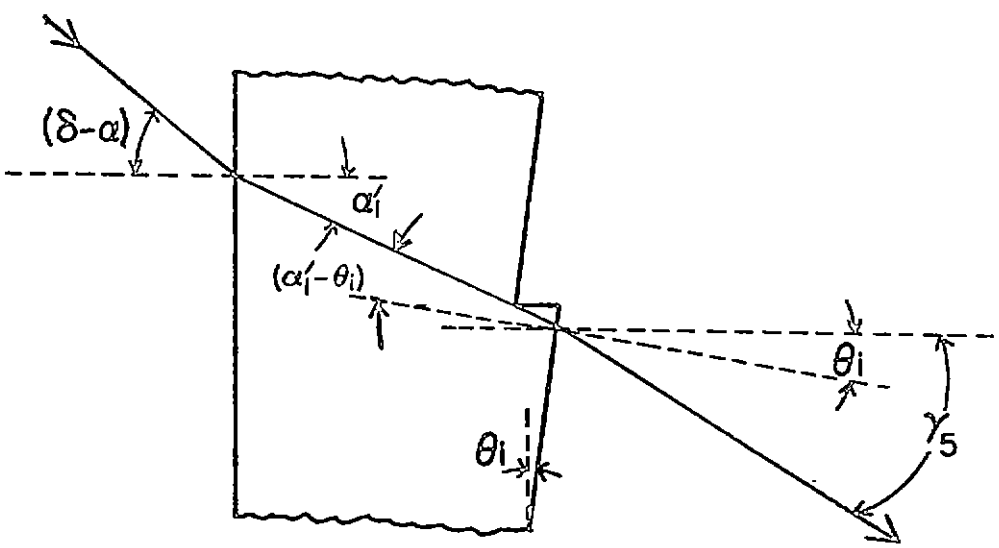

(b)

Figure 6. Y_r extreme ray paths in lower lens half serrations; $\delta \geq \alpha$.

The case in Figure 6(b) may occur for small groove angles and the results are also described by Equations (44) thru (47).

Rays determining Y_ℓ are depicted in Figure 7(a), (b), and (c). Using the sketch in (a),

$$Y_{\ell b} = - \left[y_i + \frac{(\Delta y)_i}{2} - (f + \Delta\ell - t)\tan \gamma_6 \right] , \qquad (48)$$

where

$$\gamma_6 = \text{Arcsin}[n \sin(\theta_i - \alpha_2')] - \theta_i . \qquad (49)$$

For the cases in Figure 7(b) and (c),

$$Y_{\ell b} = - \left[y_i + \frac{(\Delta y)_i}{2} - \left[f + \Delta\ell - t - (\Delta y)_i \tan \theta_{i+1} \right] \tan \gamma_6 \right] . \qquad (50)$$

b. $\delta < \alpha$

For an error angle less than the half angle subtended by the sun and for serrations in the lens lower half, the ray shown in Figure 8 determines the intercept position Y_{rb}:

$$Y_{rb} = - \left[y_i - \frac{(\Delta y)_i}{2} - \left[f + \Delta\ell - (\Delta y)_i \tan \theta_i \right] \tan \gamma_7 \right] \qquad (51)$$

where

$$\gamma_7 = \text{Arcsin}[n \sin (\theta_i + \alpha_3')] - \theta_i . \qquad (52)$$

The intercept $Y_{\ell b}$ is defined thru Figure 7 and Equations (48) thru (50).

Using Equations (32) thru (52), the beam spread width L for sunlight with wavelength λ_j and refracted by any serration may be computed. Summing over all wavelengths and serrations in Equation (31) yields the intensity profile in the chosen intercept plane.

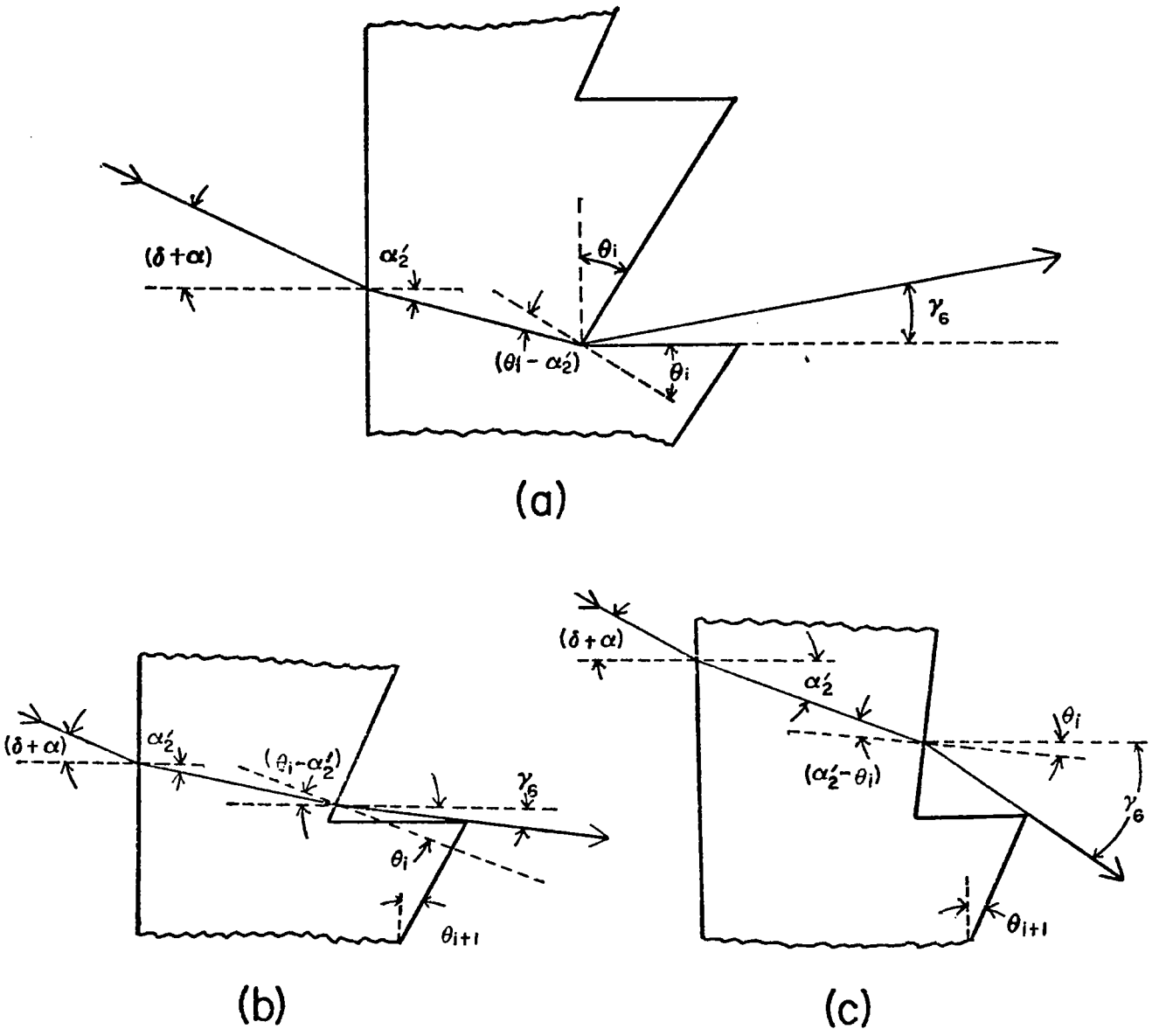

Figure 7. Y_{ℓ} extreme ray paths in lower lens half serrations; $\delta \geq \alpha$.

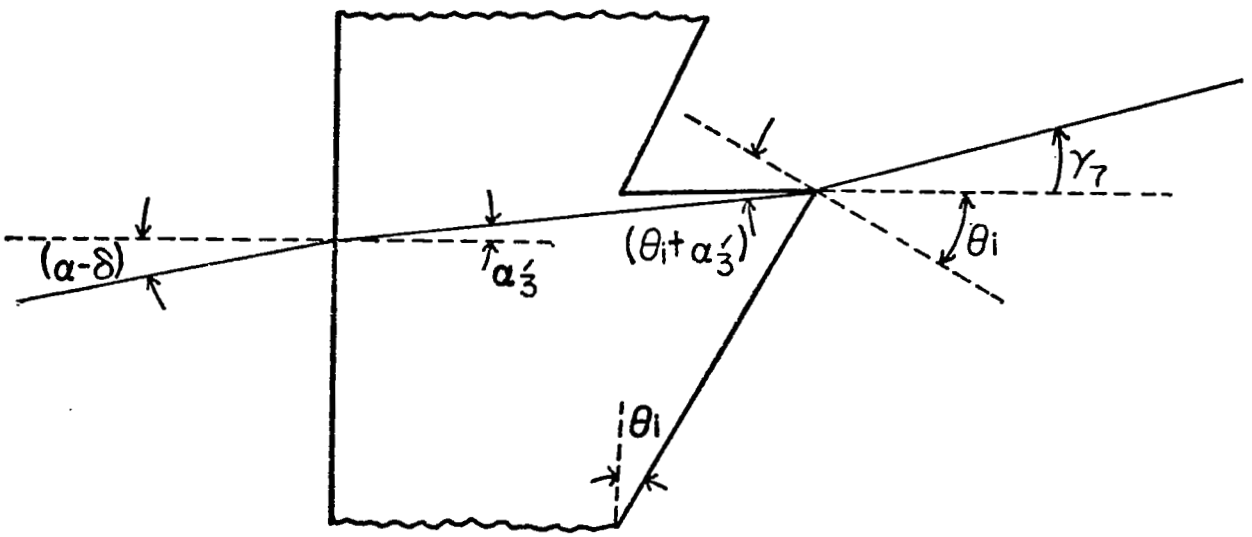

Figure 8. Y_r extreme ray path in lower lens half serrations; $\delta < \alpha$.

III. THEORETICAL RESULTS

Based on the preceding theoretical model, a computer program was developed to provide example performance data. Lens parameters were selected to correspond with existing experimental concentrators (Tables 1 and 2) to facilitate comparisons of analytical/experimental results. Performance data for other lens sizes may be approximately determined by using appropriate scaling factors.

For the computations, the solar spectrum proposed by Moon [4] as a standard solar radiation curve was incremented as illustrated in Table 3 and appropriate weighting factors assigned. Bulk transmittance factors for acrylic were determined by the method outlined in [1] and are also listed in Table 3 along with the indices of refraction obtained from manufacturer's data [5].

With these input parameters and data, the lens transmission and focal plane solar images were studied as a function of transverse tracking error up to 2.5° for the 56 cm lens and 0.75° for the 1.8 m lens.

A. Example Data - 0.56 Meter Test Lens

1. Lens Transmission

Total lens sunlight transmittance was practically unaffected by the presence of a small transverse tracking error. The computed transmittance decreased by less than 1% (from 87.4 to 86.6%) as the tracking error was increased from 0° to 2.5°. The decrease may be attributed to groove edge losses and to increased reflection losses for upper half grooves. As illustrated in Table 4, higher transmission for lower half serrations partially compensates for the increased upper half reflection losses. The changes in transmission for the two lens halves with respect to the zero tracking error case are illustrated by the data. In general,

TABLE 1. TEST LENS CHARACTERISTICS

Lens Type	Cylindrical Fresnel, Grooves Down
Material	Rohm and Haas Plexiglas VS
Fabrication Technique	Compression Molding
Manufacturer	Optical Sciences Group, Inc.
f-number	1.0
Center Thickness	0.434 cm (0.171 in.)
Groove Density	13.58/cm (34.5/in.)
Design Wavelength	5893 Å

TABLE 2. LARGE TEST LENS CHARACTERISTICS

Lens Type	Cylindrical Fresnel, Grooves Down
Material	Rohm and Haas Plexiglas V(811)
Fabrication Technique	Compression Molding
Manufacturer	Optical Sciences Group, Inc.
Width	182.9 cm (72 in) Active Aperture 186.7 cm (73.5 in) Total Aperture
Focal Length (for design wavelength)	168.0 cm (66.15 in)
Geometric F-Number	0.9
Center Thickness	0.594 cm (0.234 in)
Groove Density	8.8 cm^{-1} (inner 18 inch panel) 13.2 cm^{-1} (outer 18 inch panel)
Design Wavelength	625 nanometers

TABLE 3. SOLAR AND LENS SPECTRAL PARAMETERS

Wavelength Increment $(\Delta\lambda)_j$ (microns)	Center Wavelength λ_j (microns)	Weighting Factors ω_j	Acrylic Index of Refraction n_j		Acrylic Bulk Transmittance Factor $(T_a)_j$	
0.295-0.40	0.374	2.67×10^{-2}	1.5250	(estimate)	0.962	(0.675)†
0.40-0.43	0.416	2.75	1.5155		1	(0.995)†
0.43-0.45	0.441	2.44	1.5018		1	
0.45-0.47	0.460	2.91	1.4999		1	
0.47-0.49	0.480	3.20	1.4982		1	
0.49-0.51	0.500	3.27	1.4968		1	
0.51-0.53	0.520	3.23	1.4954		1	
0.53-0.55	0.540	3.22	1.4942		1	
0.55-0.57	0.560	3.19	1.4930		1	
0.57-0.60	0.585	4.73	1.4918		1	
0.50-0.63	0.615	4.73	1.4906		1	
0.63-0.66	0.645	4.75	1.4895		1	
0.66-0.69	0.675	4.56	1.4886		1	
0.69-0.73	0.709	5.37	1.4876		1	
0.73-0.78	0.753	5.91	1.4865		1	
0.78-0.83	0.804	5.62	1.4854		1	
0.83-0.89	0.857	6.23	1.4845		1	
0.89-0.99	0.953	6.06	1.4832		1	
0.99-1.06	1.024	5.65	1.4826		1	
1.06-1.21	1.129	6.21	1.4818		0.948	
1.21-1.52	1.274	6.49	1.4812	(estimate)	0.912	
1.52-2.2	1.642	6.81	1.4808	(estimate)	0.570	

†Values in parentheses used for 1.8 m lens computations.

TABLE 4. COMPUTED SUNLIGHT TRANSMITTANCE OF TEST LENS SERRATIONS; 0.56 M LENS

Serration Number	Serration Position y_i/W	Sunlight Transmittance		
		$\delta = 0°$ (Each Lens Half)	$\delta = 2.5°$ Lens Half	
			Upper	Lower
0	6.494×10^{-4}	.8878	.8878	.8878
20	2.662×10^{-2}	.8878	.8864	.8485
40	5.260×10^{-2}	.8878	.8850	.8878
60	7.857×10^{-2}	.8877	.8836	.8878
80	.1045	.8875	.8821	.8878
100	.1305	.8873	.8805	.8876
120	.1565	.8869	.8787	.8874
140	.1825	.8862	.8766	.8869
160	.2084	.8852	.8741	.8863
180	.2344	.8839	.8711	.8853
200	.2604	.8820	.8675	.8840
220	.2864	.8795	.8631	.8822
240	.3123	.8763	.8578	.8800
260	.3383	.8724	.8512	.8772
280	.3643	.8675	.8434	.8739
300	.3903	.8616	.8338	.8699
320	.4162	.8546	.8224	.8653
340	.4422	.8464	.8086	.8600
360	.4682	.8369	.7921	.8540
380	.4942	.8260	.7723	.8473

TABLE 5. LENS TRANSMITTANCE OVER THE SOLAR SPECTRUM FOR A TRANSVERSE TRACKING ERROR OF 1.5°; 0.56 M LENS

Wavelength Increment $(\Delta\lambda)_j$ (microns)	Transmittance	Wavelength Increment $(\Delta\lambda)_j$ (microns)	Transmittance
0.295-0.40	0.8592	0.63-0.66	.9058
0.40-0.43	.9002	0.66-0.69	.9061
0.40-0.45	.9016	0.69-0.73	.9065
0.45-0.47	.9022	0.73-0.78	.9068
0.47-0.49	.9028	0.78-0.83	.9072
0.49-0.51	.9033	0.83-0.89	.9075
0.51-0.53	.9038	0.89-0.99	.9079
0.53-0.55	.9042	0.99-1.06	.9081
0.55-0.57	.9046	1.06-1.21	.8611
0.57-0.60	.9050	1.21-1.52	.8286
0.60-0.63	.9054	1.52-2.2	.5180

Total sunlight transmittance = 0.8702

transmittance decreases with increasing serration distance from the lens center, as illustrated in Figure 9 for a 1.5° tracking error, due to the larger groove angles and hence increased angles of incidence. A tracking error increases the angles of incidence at the grooved surface for the upper lens half and decreases these angles for the lower half.

Groove edge losses result in a reduced transmittance but are of minor importance for the small tracking errors considered. For upper half serrations, edge losses increase monotonically from near zero for the center serration to, typically, 1 to 2% for the outermost serration; e.g., at 1.5° tracking error the maximum loss is 1.33%. For the lower half and $\delta > \alpha$, blocking losses occur only for serrations with small groove angles. Figures 3(a) and 3(b) illustrate the blocking mechanisms responsible for the transmittance "dip" near the lens center shown in Figure 9 for a tracking error of 1.5°. These blocking mechanisms cease to function when the groove angle becomes sufficiently large.

Table 5 lists the lens transmittance for each of the 22 intervals of the solar spectrum used in the computations. Absorption in the lens material occurs primarily in the infrared region of the solar spectrum. For example, high absorption drops the transmittance in the spectral range 1.52-2.2 microns from above 90% to below 52%. The reflection losses are seen to decrease only very slowly with wavelength.

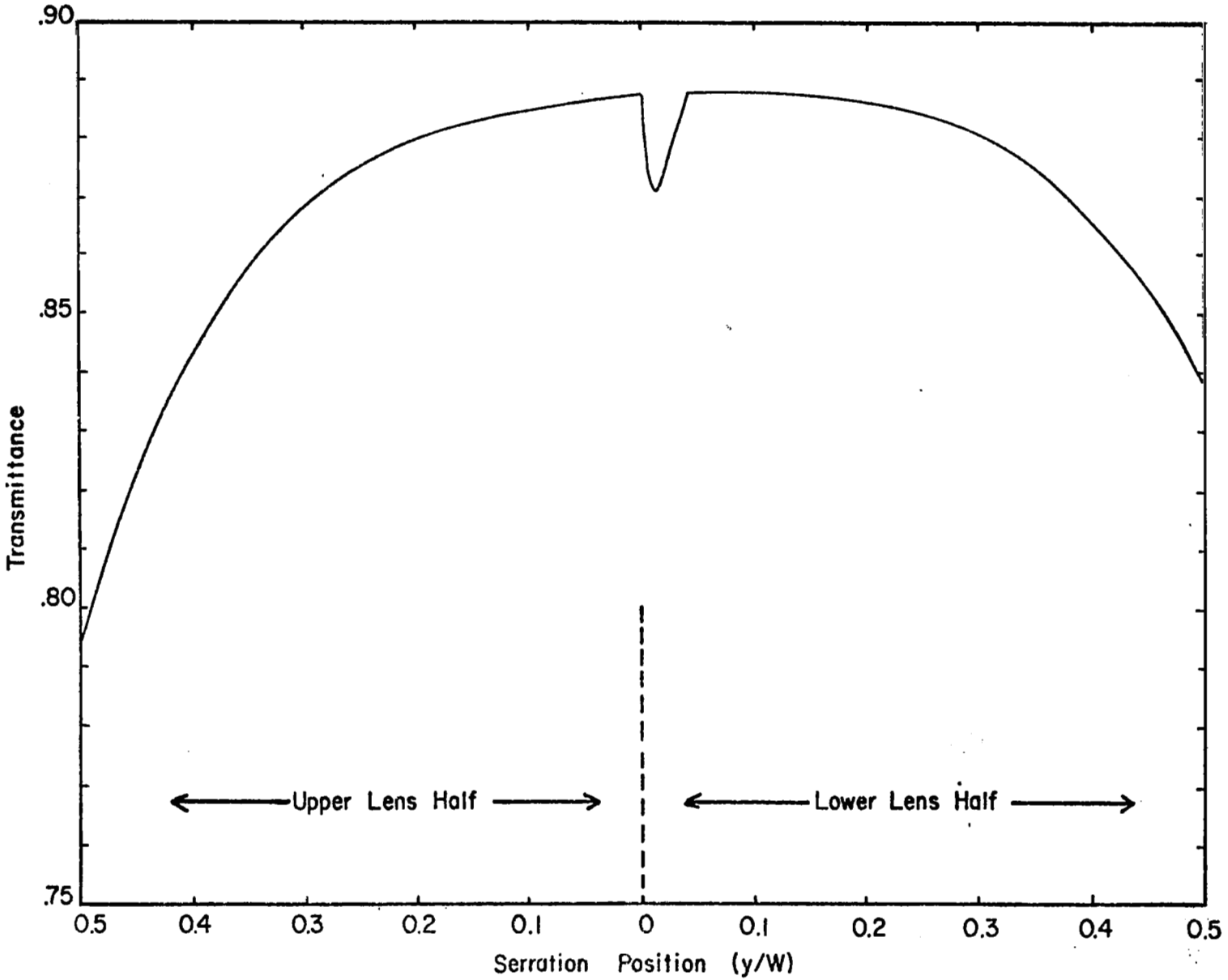

Figure 9. Transmittance versus serration position for $\delta = 1.5°$; 0.56 m lens.

2. Focal Plane Intensity Profiles

The local concentration ratio as a function of focal plane position has been computed for the test lens for transverse tracking errors in the range 0° - 2.5°. Figures 10 and 11 depict the computed intensity profiles. The presence of a tracking error modifies the distribution of concentrated sunlight by (1) laterally shifting the profile, (2) generally reducing the peak concentration, and (3) altering the profile symmetry.

The lateral shifting of the profile is quantified in Figure 12 by plotting the peak position shift as a function of orientation error. The shift increases approximately linearly over the range examined and may be compared with the image displacement $\delta \times f$ expected for a monochromatic point source.

The change in the focal plane peak concentration with increasing tracking error is depicted in Figure 13 . For a small misalignment angle larger than α and for this particular intercept plane, the computed peak concentration is greater than the zero tracking error case, but then monotonically decreases as the error increases. For $\delta < \alpha$, the peak concentration remains nearly constant.

Profile asymmetry becomes conspicuous for the larger tracking errors, with a long "tail" developing in a direction away from the focal line. This redistribution of energy simultaneously sharpens the profile on the other side.

Increasing profile shift and skewness with tracking error result in large increases in the target width designed to intercept an acceptable fraction of the concentrated energy. The target widths required for 90% interception beneath concentrators with tracking systems whose design tolerances are $\pm \delta$ are illustrated in Figure 14 . As an example, for

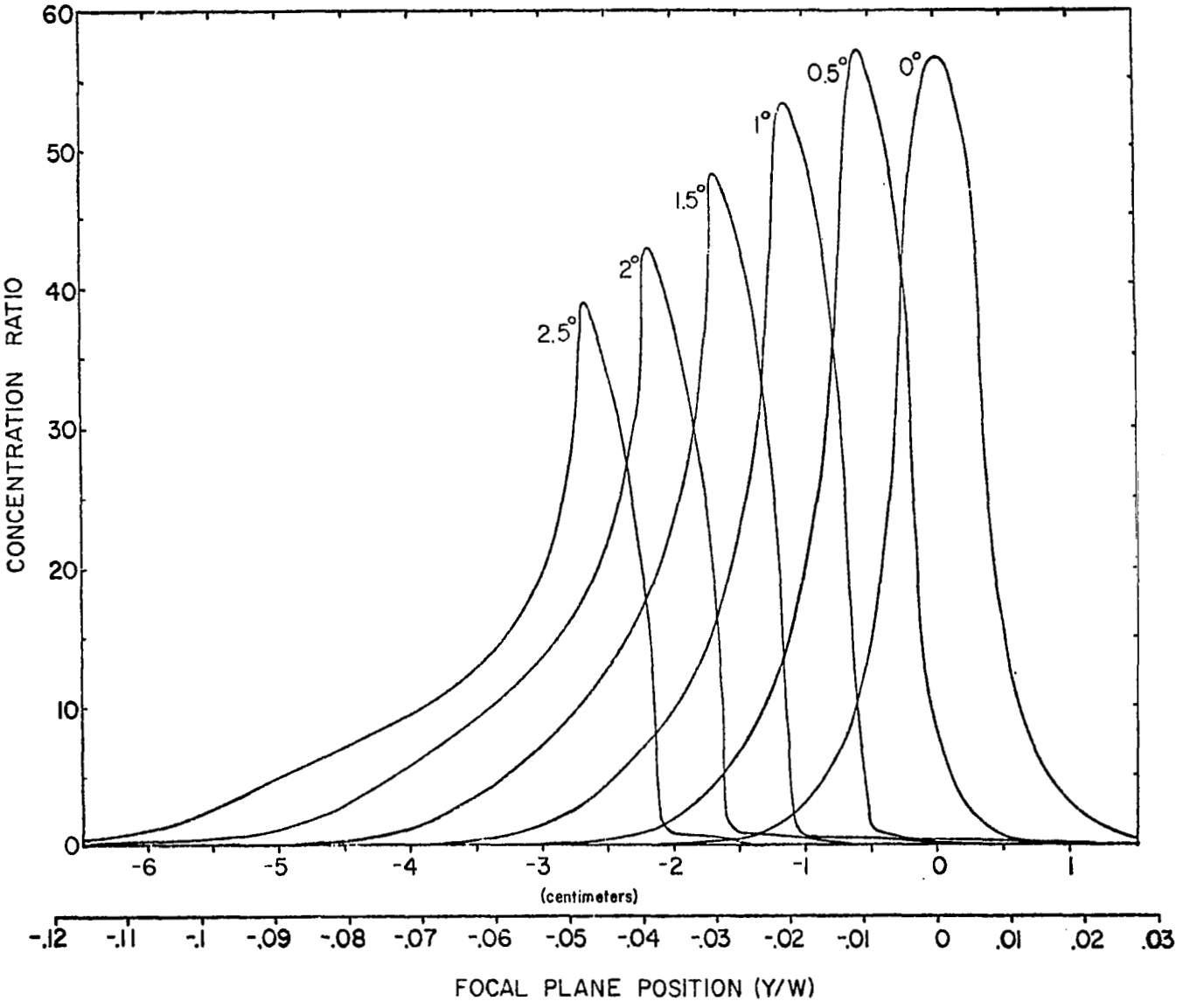

Figure 10. Transverse orientation effects on intensity profile; 0.56 m lens.

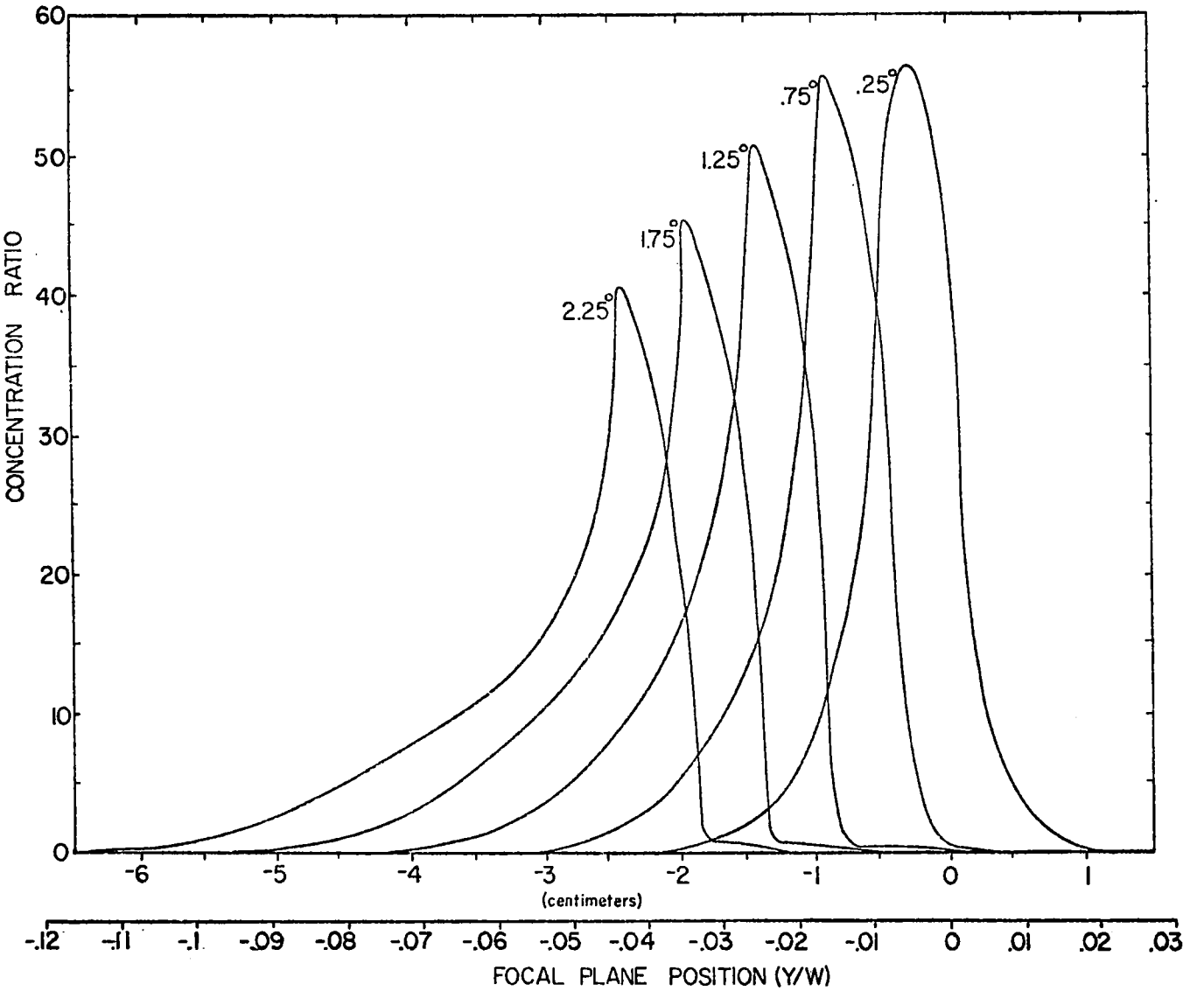

Figure 11. Transverse orientation effects on intensity profile; 0.56 m lens.

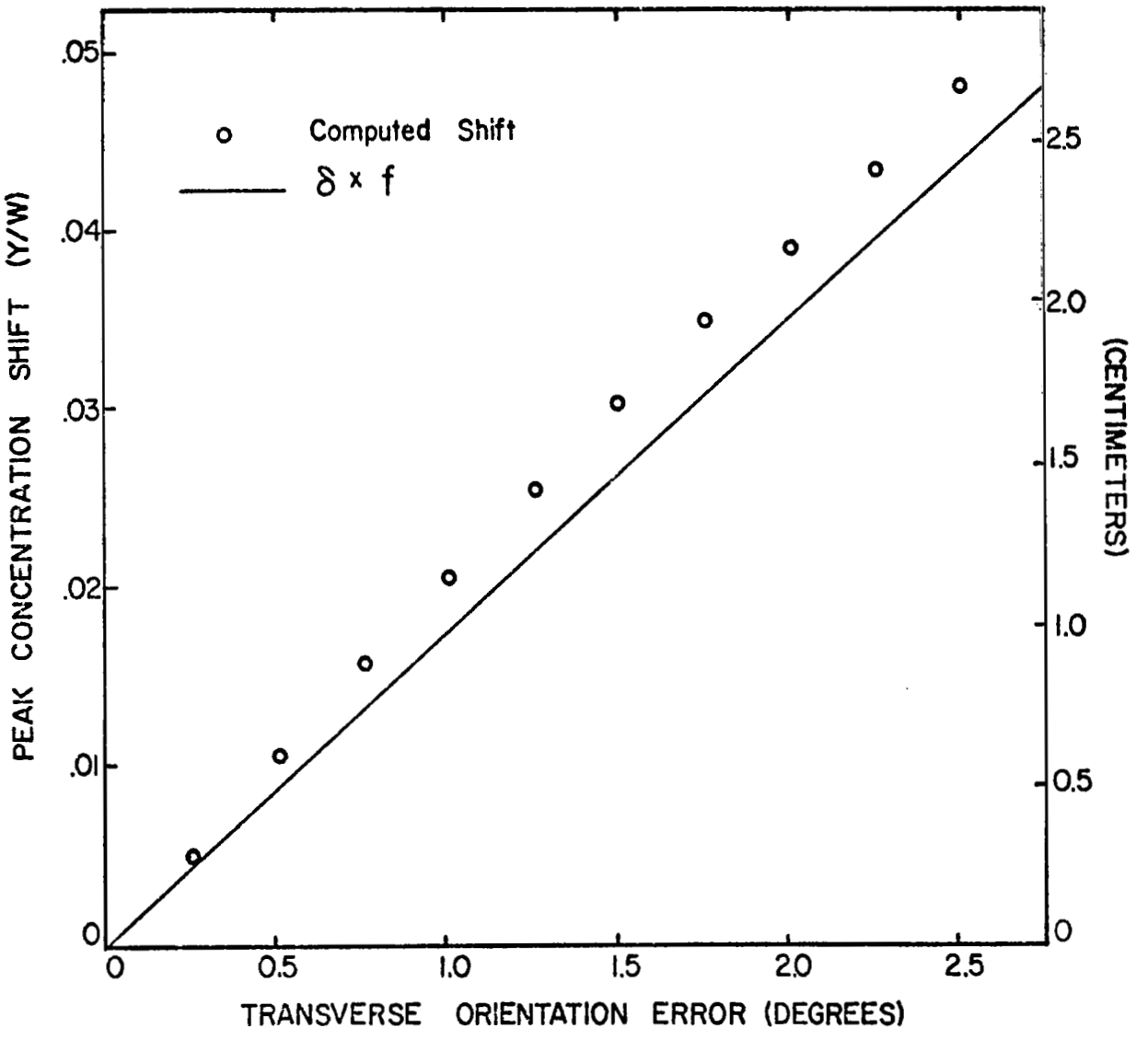

Figure 12. Transverse orientation effects on profile position; 0.56 m lens.

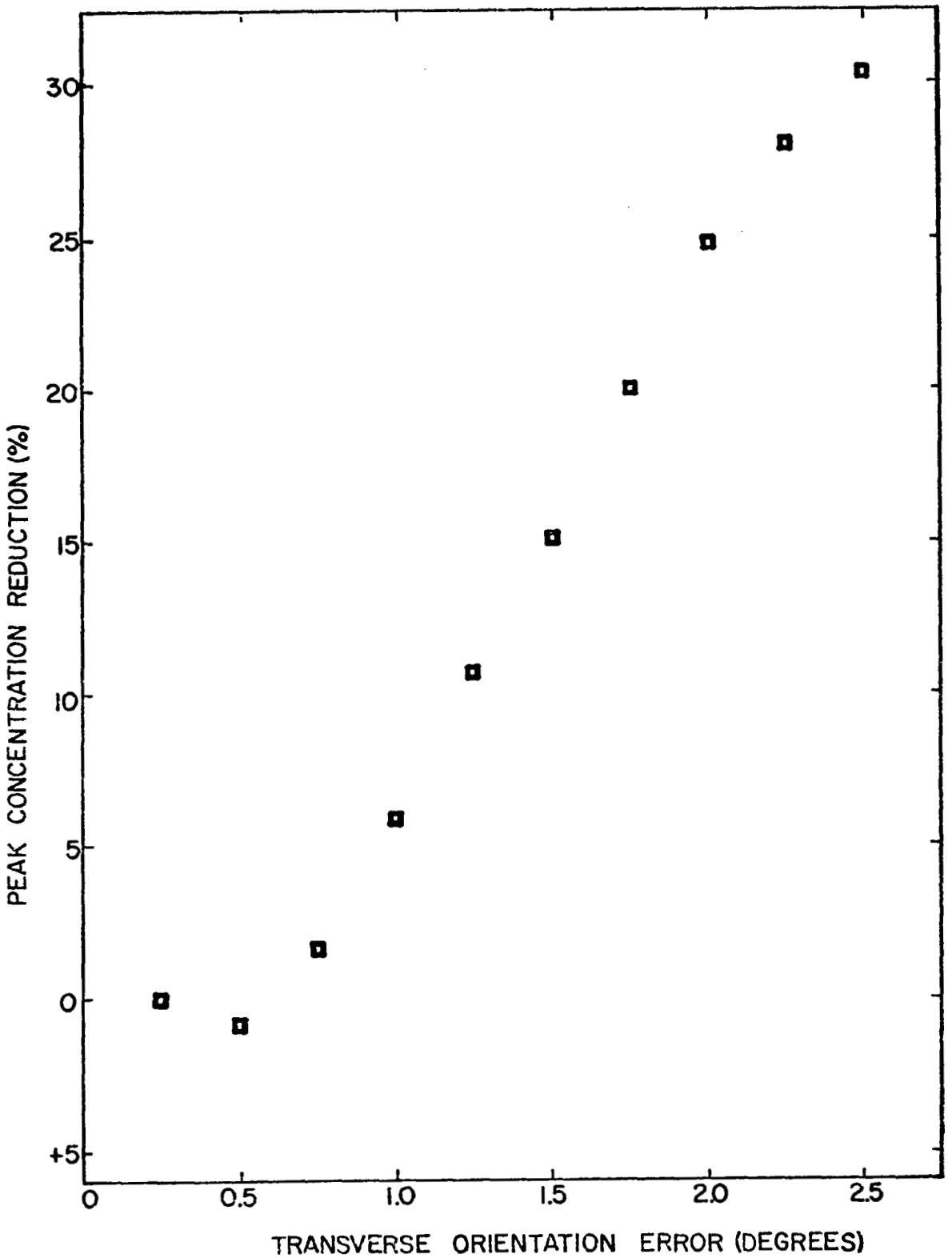

Figure 13. Transverse orientation effects on peak concentration; 0.56 m lens.

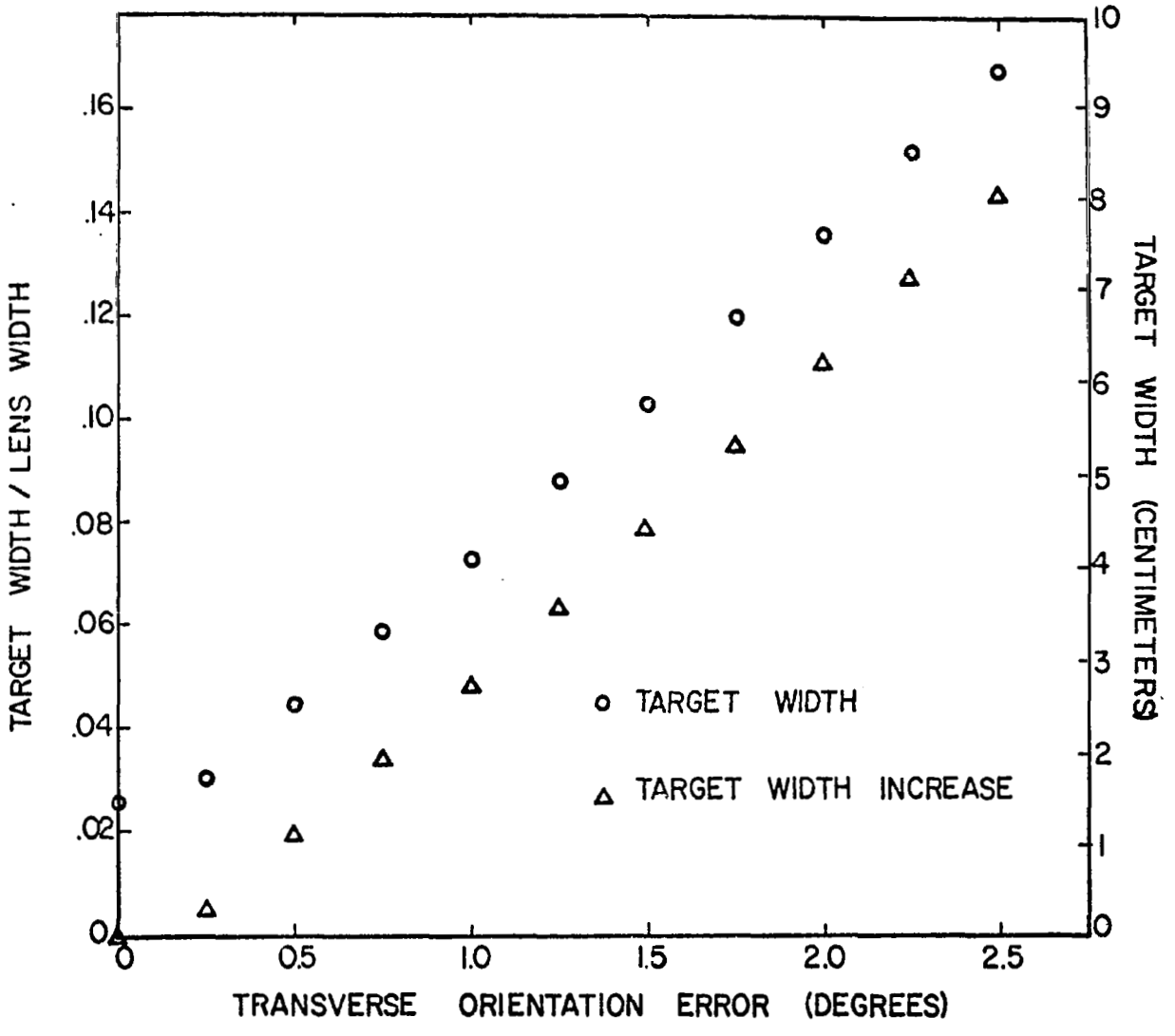

Figure 14. Transverse orientation effects on target width; 0.56 m lens.

$\delta = \pm 1°$, a three-fold increase in target width over the perfect alignment case is computed for the test lens (4.1 cm vs 1.4 cm). Profile shift is responsible for most of this increase. If the zero misalignment profile is simply shifted to the 1° profile peak position, the change in the target width represents roughly 70% of the increase computed for the 1° profile. For larger tracking errors, the importance of profile skewness grows.

B. Example Data - 1.8 Meter Test Lens

The transmitted fraction of sunlight striking the total lens aperture was computed to be 0.842 for a flawlessly tracking lens. The transmittance dropped by less than two-tenths of one per cent for transverse deviations up to 0.75°.

Focal plane image profiles were determined for errors of 0, 0.15, 0.26, 0.52, and 0.75° (Figure 15). These profiles exhibit similar characteristics with respect to peak shift (Figure 16), peak concentration reduction (Figure 17), and skewness as in the previous example. Again, substantial increases with tracking error are observed in the target width required to intercept 90% of the transmitted flux (Figure 18). For example, for a lens concentrator system designed to track the center of the sun within ±0.25°, the aperture of the secondary concentrator or absorber must be increased in width by approximately one third over that required for the flawless tracking case.

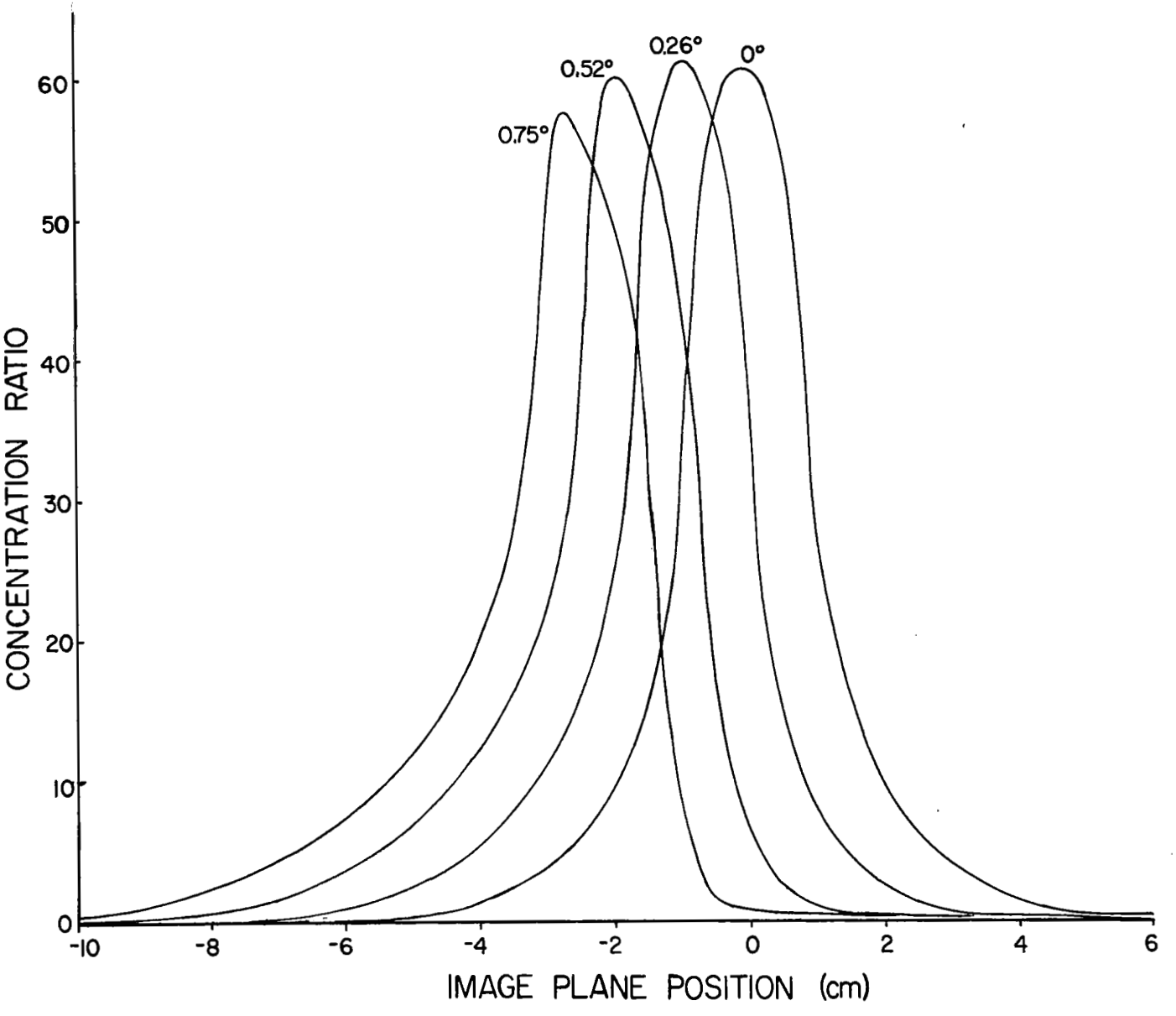

Figure 15. Transverse orientation effects on intensity profile; 1.83 m lens.

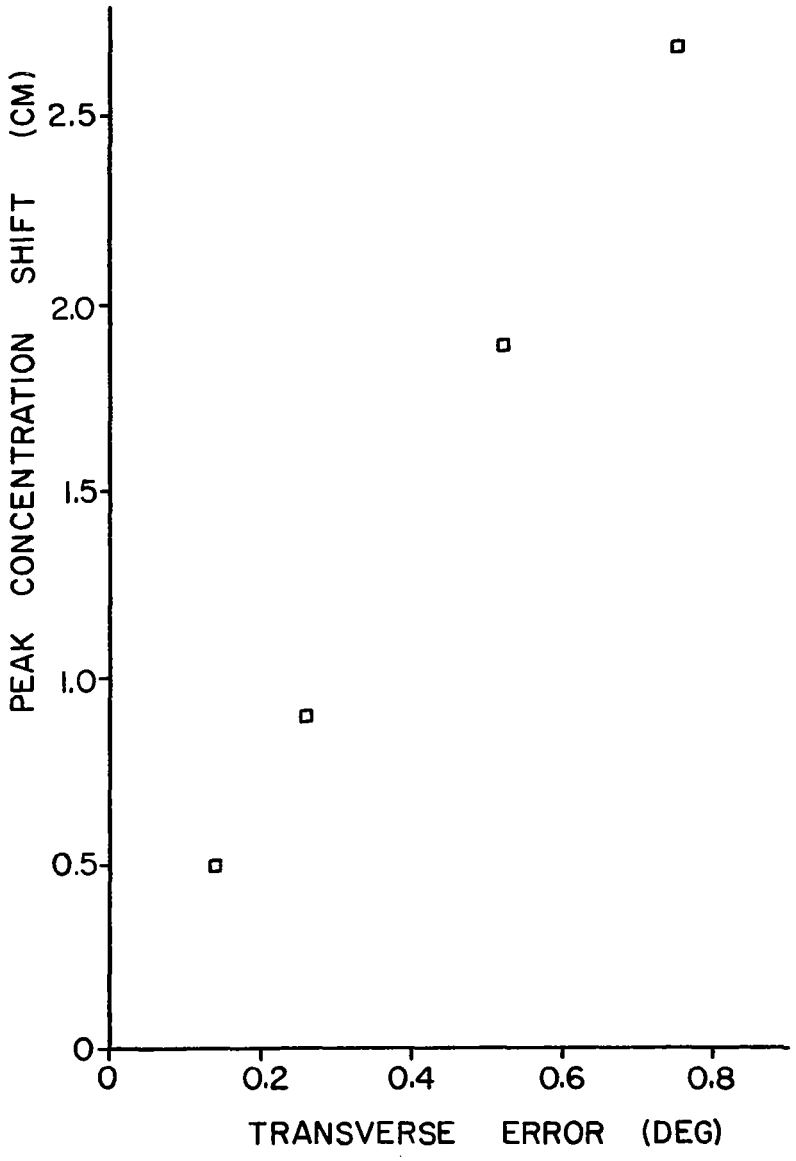

Figure 16. Transverse orientation effects on profile peak position; 1.83 m lens.

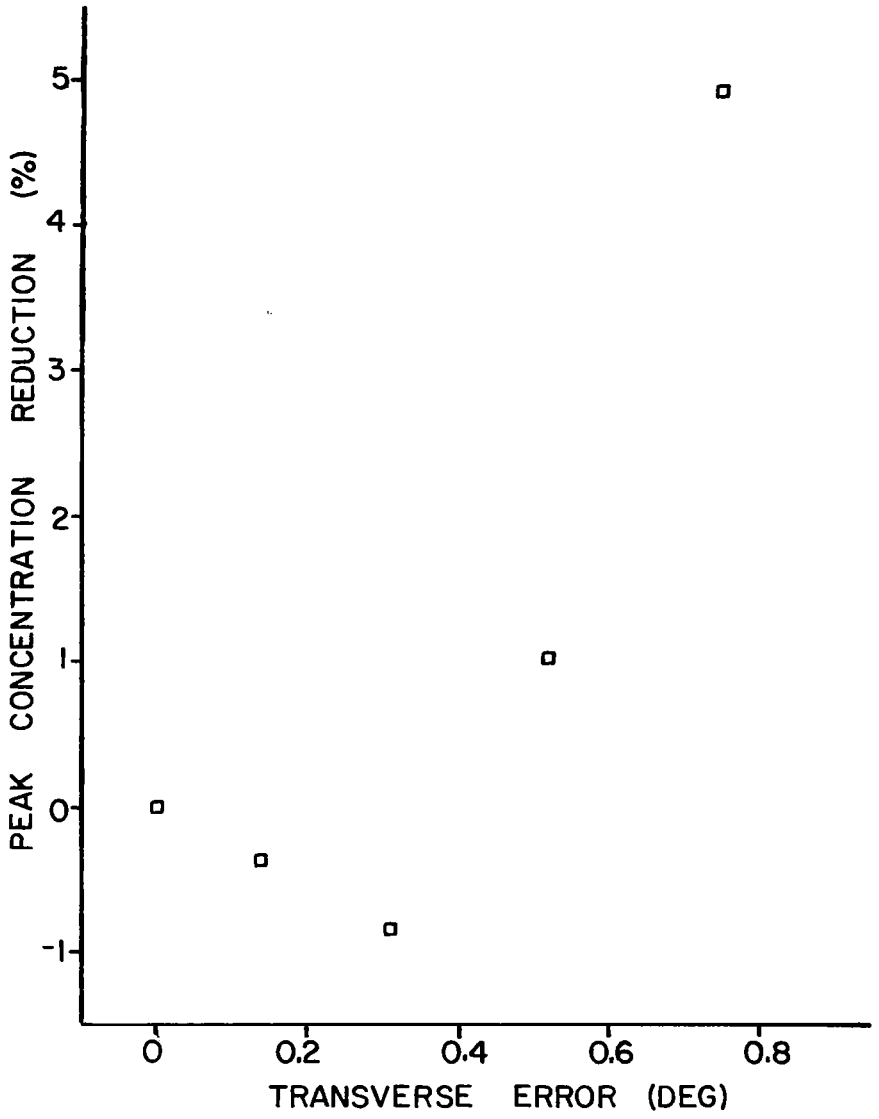

Figure 17. Transverse orientation effects on peak concentration; 1.83 m lens.

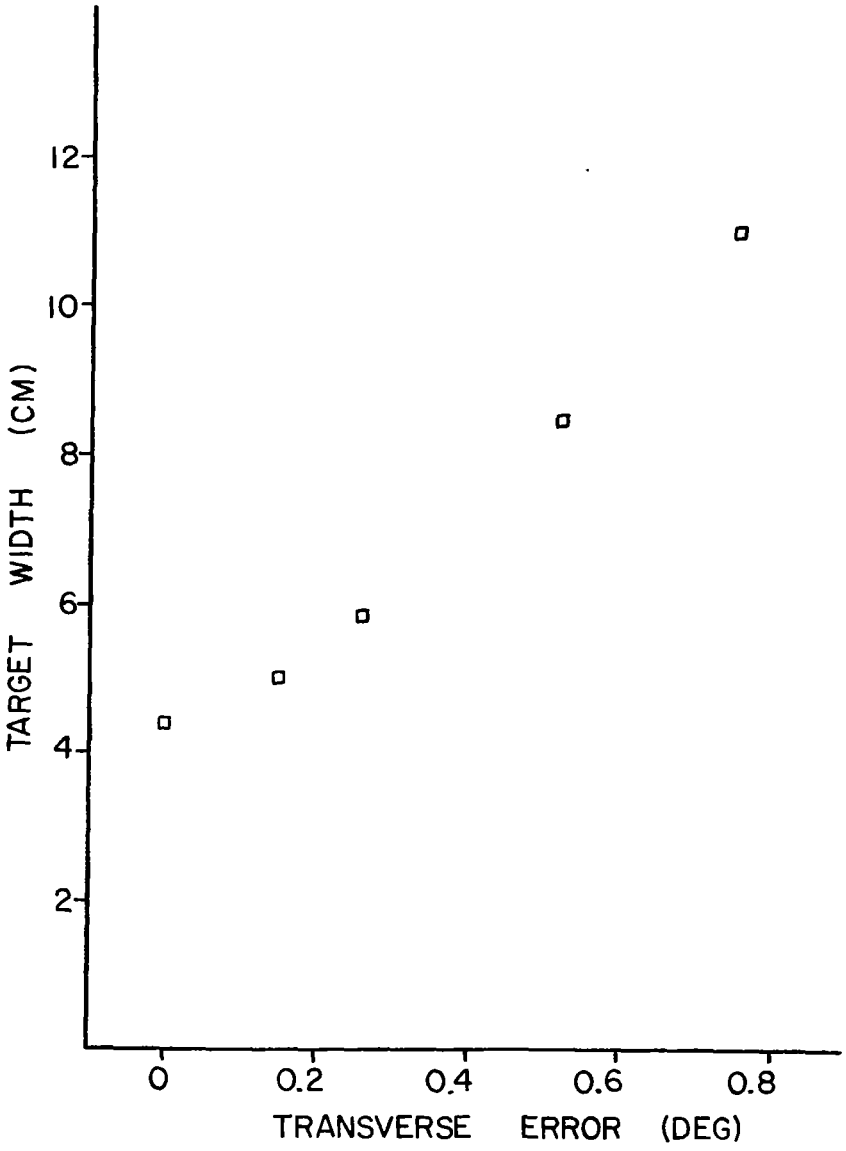

Figure 18. Transverse orientation effects on target width; 1.83 m lens.

IV. SUMMARY AND CONCLUSIONS

1. An optical ray trace analysis for assessing small (<5°) transverse tracking error effects on the solar transmission and imaging properties of a linear Fresnel lens was developed. In addition to tracking error, variable parameters include intercept plane position and such lens characteristics as f-number, groove density, and design index of refraction.
2. Transmittance and image profile computations were performed for a 56 cm wide, f/1.0 and a 1.83 m, f/0.9 test lens to provide a data base for comparison with experimental data from NASA test programs.
3. Lens transmittance is only slightly degraded (<1%) for misalignments up to 2.5°.
4. Solar image degradation with tracking error includes an approximately linearly dependent profile shift, a peak concentration reduction, and increased profile skewness.
5. The 90% target intercept width increases rapidly for small transverse tracking errors, almost threefold for a 1° error over the perfect tracking case for the small test article, and at a similar rate for the large lens.
6. The primary cause for target width increases in the presence of transverse tracking errors is profile shift.
7. The theory and results in this study provide an analytical base, albeit approximate, for the design of the interrelated tracking and target absorber systems for a flat linear Fresnel lens solar concentrator.

V. REFERENCES

1. L. Hastings, S. Allums, and R. Cosby, "An Analytical and Experimental Evaluation of a Fresnel Lens Solar Concentrator", NASA Technical Memorandum TM X-73333, August, 1976.

2. L. Hastings, S. Allums, and R. Cosby, "An Analytical and Experimental Evaluation of the Plano-Cylindrical Fresnel Lens Solar Concentrator", Proceedings of the "Sharing the Sun" Joint Conference of the American, Canadian, and International Solar Energy Society, Winnepeg, Canada. Vol. 2, (August 1976), p. 275.

3. R. Cosby, "Concentration Characteristics of the Cylindrical Fresnel Lens Solar Concentrator", in 1975 NASA-ASEE Summer Faculty Fellow Research Reports, BER Report No. 202-94, (George C. Marshall Space Flight Center/University of Alabama/ Auburn University), September, 1975, p. III-1.

4. P. Moon, "Proposed Standard Solar-Radiation Curves for Engineering Use", J. Franklin Institute, 23a, 583 (1940).

5. Rohm and Haas Company, Philadelphia, PA, "Plexiglas Injection and Extrusion Molding Powders," Publication PL 165f, December 1968.

APPENDIX

GROOVE BLOCKING LOSSES

Assuming all solar rays striking a groove edge are lost, the problem is to calculate, for a given small tracking error, the average fraction of incident rays on a serration which are blocked from reaching the solar image. Noting our approximation of zero ray axial components, each case illustrated in Figures 2(a), (b), (c) and Figures 3(a), (b), (c) must be evaluated separately.

CASE: Figure A1(a), upper half.

Redrawing the ray diagram of Figure 2(a) to provide more detail, it is observed that the lost fraction of rays incident at an angle ϕ_i on the serration of width Δy is

$$F = \frac{s}{\Delta y} \quad . \tag{A-1}$$

Now

$$s = \Delta t \tan\phi_t \ , \tag{A-2}$$

where

$$\Delta t = \Delta y \tan \Theta_i \ . \tag{A-3}$$

Then

$$s = \Delta y \tan \Theta_i \tan \phi_t \quad . \tag{A-4}$$

Using Snell's law of refraction,

$$\tan\phi_t = \frac{\sin\phi_i}{\sqrt{n^2 - \sin^2\phi_i}} \tag{A-5}$$

Combining Equations (A-1) thru (A-5).

$$F(\phi_i) = \tan\Theta_i \frac{\sin\phi_i}{\sqrt{n^2 - \sin^2\phi_i}} \quad . \tag{A-6}$$

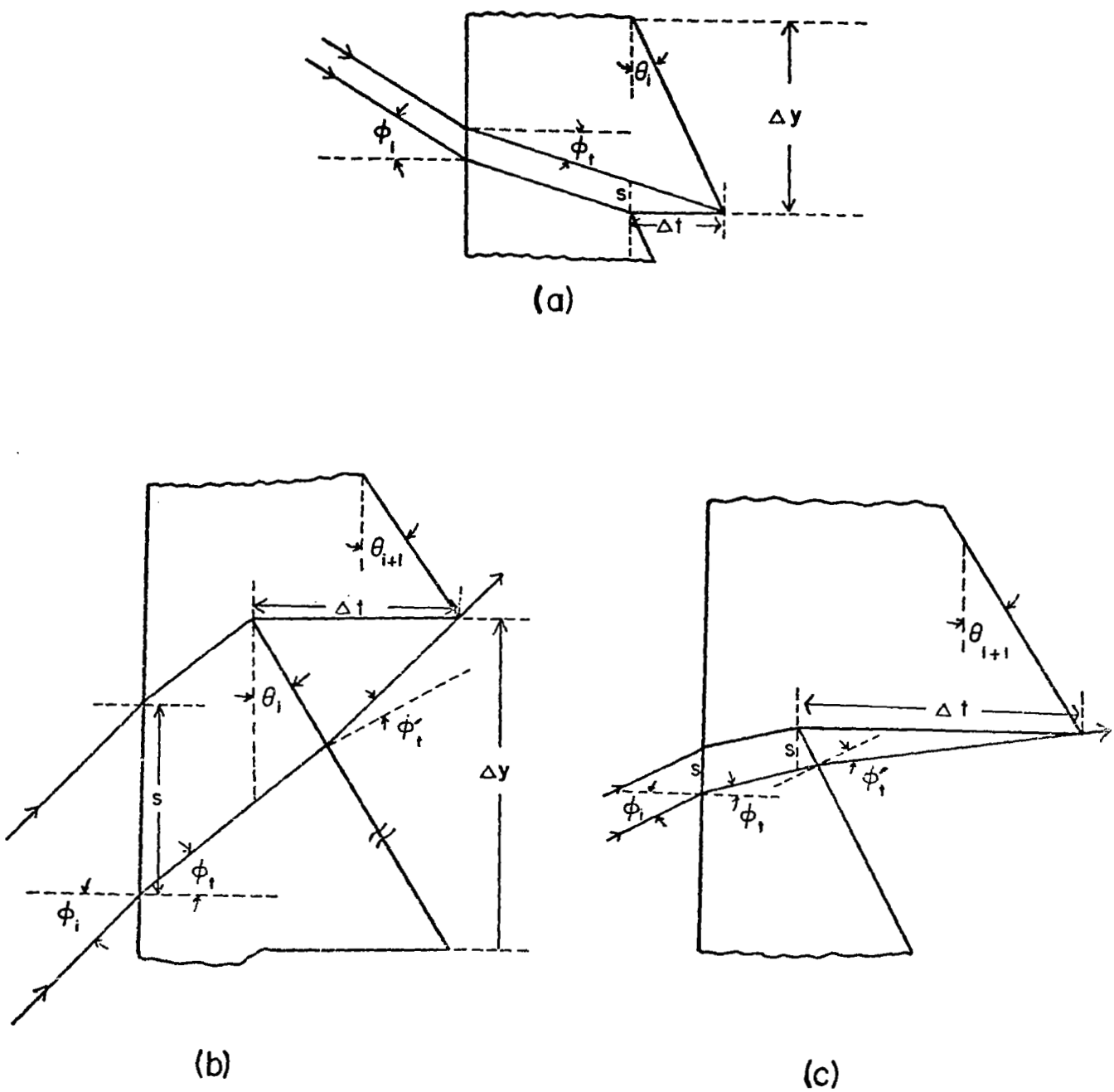

Figure A1. Ray diagrams for groove edge losses in upper lens half.

For a tracking error δ, the average fraction lost is

$$F_u' = \frac{\int F(\phi_i)\, d\phi_i}{\int d\phi_i} \qquad \text{(A-7)}$$

$$= \tan \Theta_i \frac{\int_{\phi_o}^{\delta+\alpha} \frac{\sin \phi_i \, d\phi_i}{n^2 - \sin^2 \phi_i}}{\int_{\delta-\alpha}^{\delta+\alpha} d\phi_i} \quad ,$$

where $\phi_o = \delta - \alpha$ if $\delta > \alpha$ and $\phi_o = 0$ if $\delta < \alpha$.

Assuming small tracking errors, $\sin \phi_i \simeq \phi_i$, and the integral simplifies to

$$F_u' \simeq \frac{\tan \Theta_i}{2\alpha} \int_{\phi_o}^{\delta+\alpha} \frac{\phi_i \, d\phi_i}{\sqrt{n^2 - \phi_i^2}} \, . \qquad \text{(A-8)}$$

Evaluation of this simple integral yields

$$F_u' \simeq \frac{\delta \tan \Theta_i}{n} \quad , \quad \delta \geq \alpha \quad ; \qquad \text{(A-9)}$$

and

$$F_u' \simeq \frac{(\delta + \alpha)^2 \tan \Theta_i}{4\alpha n} \quad , \quad \delta < \alpha \, . \qquad \text{(A-10)}$$

CASE: Figure A1(b), upper half.

Referring to the diagram, it is clear that in this case, blocking losses can occur only if $\delta < \alpha$ and when the angle of refraction at the first surface is greater than or equal to Θ_i, requiring

$$\phi_i > \text{Arcsin}(n \sin \Theta_i). \qquad \text{(A-11)}$$

(Here Θ_i is the groove angle for the ith serration while ϕ_i is the angle of incidence. Thus the subscripts have different meanings.) Since for this case ϕ_i has a maximum value of α (when $\delta = 0$), these conditions are possible only for small Θ_i, i.e., only for a few of the grooves, if any,

near the lens center. Hence the losses are expected to be inconsequential.

From Figure A1(b), twice using the triangle law of sines, and recognizing that

$$\Delta t \approx \Delta y \tan \Theta_{i+1} \quad , \tag{A-12}$$

the lost fraction for rays with angles of incidence ϕ_i is

$$F(\phi_i) = \frac{s}{\Delta y} = \left[\frac{\tan \Theta_{i+1} \sin(\Theta_i + \phi_t') \cos(\phi_t - \Theta_i)}{\cos \phi_t' \cos \phi_t} \right] . \tag{A-13}$$

Applying Snell's law of refraction at the two lens surfaces and using the fact that ϕ_i and Θ_i are very small,

$$\phi_t \approx \frac{\phi_i}{n} \quad , \tag{A-14}$$

and

$$\phi_t' \approx \phi_i - n\Theta_i \quad . \tag{A-15}$$

Further

$$\cos(\phi_t - \Theta_i) \approx \cos \phi_t' \approx \cos \phi_t \approx 1 \quad . \tag{A-16}$$

Then

$$F(\phi_i) \approx \tan \Theta_{i+1} [\phi_i - (n - 1) \Theta_i] \quad . \tag{A-17}$$

Integrating as in Equation (A-7), the average fraction of incident sunlight lost thru this blocking mechanism is

$$F_u'' \approx \frac{\tan \Theta_{i+1}}{2\alpha} \int_{\phi_o}^{\phi_f} [\phi_i - (n - 1) \Theta_i] \, d\phi_i \quad . \tag{A-18}$$

To determine the appropriate limits of integration, we note that the maximum ϕ_i is $\alpha - \delta$ and that this type of blocking does not occur if ϕ_t' in Figure A1(b), becomes zero. Thus

$$\phi_f = \alpha - \delta \quad ; \quad \phi_o = n\Theta_i \quad , \tag{A-19}$$

and proceeding with the simple integration in (A-18),

$$F_u'' \approx \frac{\tan \Theta_{i+1}}{4\alpha} [\alpha - \delta + (2 - n) \Theta_i](\alpha - \delta - n\Theta_i)$$

$$\text{for } n\Theta_i \leq \alpha - \delta \quad , \tag{A-20}$$

and obviously

$$F''_u = 0 \qquad \text{for } n\Theta_i > \alpha - \delta \ . \tag{A-21}$$

CASE: Figure A1(c), upper half.

Applying the triangle law of sines to determine s as in the previous case, the ray diagram yields

$$F(\phi_i) = \frac{s}{\Delta y} = \frac{\tan \Theta_{i+1} \sin(\Theta_i - \phi'_t) \cos(\phi_t - \Theta_i)}{\cos \phi'_t \cos \phi_t} \ . \tag{A-22}$$

Again

$$\phi_t \simeq \frac{\phi_i}{n} \ . \tag{A-23}$$

Also

$$\begin{aligned} \sin \phi'_t &\simeq n \sin(\Theta_i - \frac{\phi_i}{n}) \qquad (A\text{-}24) \\ &\simeq n \sin \Theta_i - \phi_i \cos \Theta_i \\ &= nA - B\phi_i \ , \end{aligned}$$

where

$$A \equiv \sin \Theta_i \quad ; \quad B \equiv \cos \Theta_i \ . \tag{A-25}$$

Using $\cos(\frac{\phi_i}{n}) \simeq 1$ and performing some algebraic manipulations,

$$F(\phi_i) \simeq \frac{\tan \Theta_{i+i}}{n} \left\{ nAB + A^2\phi_i - \frac{n^2AB^2 + nB(A^2 - B^2)\phi_i - AB^2\phi_i^2}{\sqrt{X}} \right\}, \tag{A-26}$$

where

$$X \equiv 1 - n^2A^2 + 2nAB\phi_i - B^2\phi_i^2 \ . \tag{A-27}$$

Now

$$F'''_u = \frac{1}{2\alpha} \int_{\phi_o}^{\phi_f} F(\phi_i) d\phi_i \ , \tag{A-28}$$

where the limits of integration for this case are

$$\phi_f = \alpha - \delta \tag{A-29}$$

$$\phi_o \simeq n\theta_i - n \arcsin\left(\frac{\sin \theta_i}{n}\right) \quad . \tag{A-30}$$

Evaluation of the integral in (A-28) using (A-25) thru (A-30) yields Equation (13) in the text of the report. For tracking errors $\delta > \alpha$, $F_u''' = 0$.

CASE: Figure A2(a), lower half of lens.

Assuming $\delta < \alpha$ and referring to the ray diagram,

$$F(\phi_i) = \frac{s}{\Delta y} = \tan \theta_i \tan \phi_t \quad . \tag{A-31}$$

Using Snell's law,

$$\tan \phi_t = \frac{\sin \phi_i}{\sqrt{n^2 - \sin^2 \phi_i}} \tag{A-32}$$

and the assumption of small δ,

$$F(\phi_i) \simeq \frac{\phi_i \tan \phi_i}{\sqrt{n^2 - \phi_i^2}} \tag{A-33}$$

Then

$$F_\ell' = \frac{\int F(\phi_i)\, d\phi_i}{2\alpha}$$

$$\simeq \frac{\tan \theta_i}{2\alpha} \int_0^{\alpha-\delta} \frac{\phi_i \, d\phi_i}{\sqrt{n^2 - \phi_i^2}} \tag{A-34}$$

Using $(\alpha - \delta) << n$,

$$F_\ell' \simeq \frac{(\alpha - \delta)^2 \tan \theta_i}{4\alpha n} \quad ; \quad \delta < \alpha \quad . \tag{A-35}$$

For $\delta > \alpha$, $F_\ell' = 0$.

CASE: Figure A2(b), lower half.

This blocking mechanism should be nontrivial only for serrations very near the lens center and for the larger tracking errors. Using

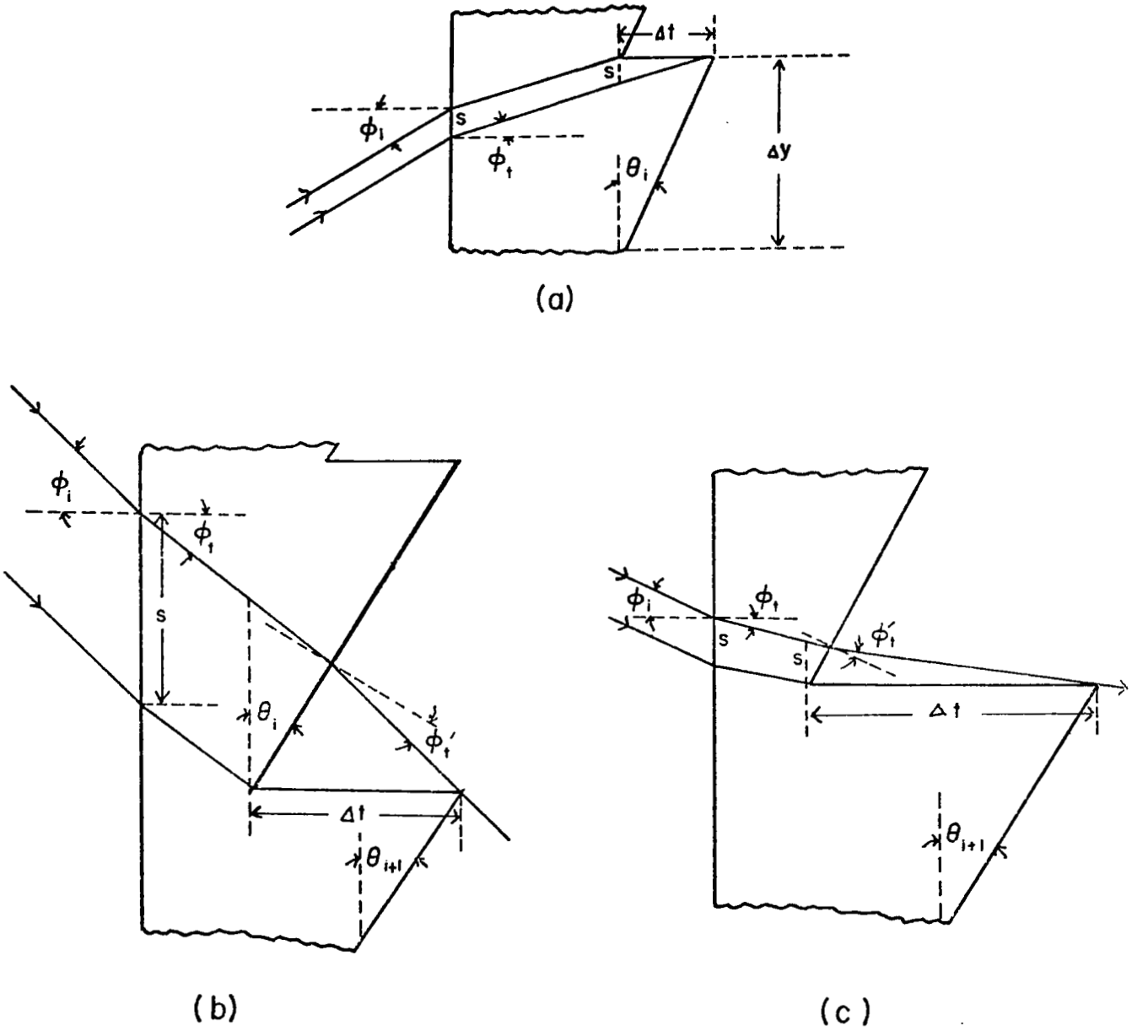

Figure A2. Ray diagrams for groove edge losses in lower lens half.

the triangle law of sines,

$$F(\phi_i) = \frac{s}{\Delta y} = \frac{\tan \Theta_{i+1} \sin(\phi_t' + \Theta_i) \cos(\phi_t - \Theta_i)}{\cos \phi_t' \cos \phi_t} \quad . \tag{A-36}$$

Again using the fact that all angles of incidence ϕ_i are very small for small δ and using Snell's laws,

$$\begin{aligned} \phi_i &\simeq n \phi_t \quad , \\ \phi_t' &\simeq \phi_i - n\Theta_i \quad . \end{aligned} \tag{A-37}$$

Then

$$F(\phi_i) \simeq \tan \Theta_{i+1} [\phi_i - (n - 1)\Theta_i] \quad . \tag{A-38}$$

Integrating over possible angles of incidence and using the limits (for serrations which have $n \Theta_i < \delta + \alpha$),

$$\phi_o \simeq n \Theta_i \quad ; \quad \phi_f = \delta + \alpha \quad , \tag{A-39}$$

$$F_\ell'' = \frac{\tan \Theta_{i+1}}{4\alpha} (\delta + \alpha - n\Theta_i)[\delta + \alpha + (2 - n)\Theta_i]. \tag{A-40}$$

CASE: Figure A2(c), lower half.

Observing the ray diagram and using the triangle law of sines,

$$F(\phi_i) = \frac{\tan \Theta_{i+1} \cos(\phi_t - \Theta_i) \sin(\Theta_i - \phi_t')}{\cos \phi_t \cos \phi_t'} \quad . \tag{A-41}$$

Noting that (A-41) is identical with (A-22), Equations (A-23) thru (A-28) are also found to apply to the present case. To determine the appropriate limits of integration for finding the average lost fraction of rays, it is noted that ϕ_o is the angle of incidence for which the emergent ray is horizontal:

$$\phi_o \simeq n \Theta_i - n \operatorname{Arcsin} \left(\frac{\sin \Theta_i}{n}\right) \quad , \tag{A-42}$$

and

$$\phi_f = n\,\theta_i \quad , \quad \text{if} \quad n\,\theta_i < \delta + \alpha \quad ; \tag{A-43}$$

$$\phi_f = \delta + \alpha \quad , \quad \text{if} \quad n\,\theta_i > \delta + \alpha \quad . \tag{A-44}$$

Evaluation of the integral in Equation (A-28) using the limits in (A-42, 43, 44) yields Equations (24) and (25) in the text of the report.

NASA-Langley, 1977